nature medicine

# A rationally designed monomeric peptide triagonist corrects obesity and diabetes in rodents

Brian Finan[1–3,11], Bin Yang[3,4,11], Nickki Ottaway[5], David L Smiley[3], Tao Ma[3,6], Christoffer Clemmensen[1,2], Joe Chabenne[3,7], Lianshan Zhang[4], Kirk M Habegger[8], Katrin Fischer[1,2], Jonathan E Campbell[9], Darleen Sandoval[5], Randy J Seeley[5], Konrad Bleicher[10], Sabine Uhles[10], William Riboulet[10], Jürgen Funk[10], Cornelia Hertel[10], Sara Belli[10], Elena Sebokova[10], Karin Conde-Knape[10], Anish Konkar[10], Daniel J Drucker[9], Vasily Gelfanov[3], Paul T Pfluger[1,2], Timo D Müller[1,2], Diego Perez-Tilve[5], Richard D DiMarchi[3] & Matthias H Tschöp[1,2]

**We report the discovery of a new monomeric peptide that reduces body weight and diabetic complications in rodent models of obesity by acting as an agonist at three key metabolically-related peptide hormone receptors: glucagon-like peptide-1 (GLP-1), glucose-dependent insulinotropic polypeptide (GIP) and glucagon receptors. This triple agonist demonstrates supraphysiological potency and equally aligned constituent activities at each receptor, all without cross-reactivity at other related receptors. Such balanced unimolecular triple agonism proved superior to any existing dual coagonists and best-in-class monoagonists to reduce body weight, enhance glycemic control and reverse hepatic steatosis in relevant rodent models. Various loss-of-function models, including genetic knockout, pharmacological blockade and selective chemical knockout, confirmed contributions of each constituent activity *in vivo*. We demonstrate that these individual constituent activities harmonize to govern the overall metabolic efficacy, which predominantly results from synergistic glucagon action to increase energy expenditure, GLP-1 action to reduce caloric intake and improve glucose control, and GIP action to potentiate the incretin effect and buffer against the diabetogenic effect of inherent glucagon activity. These preclinical studies suggest that, so far, this unimolecular, polypharmaceutical strategy has potential to be the most effective pharmacological approach to reversing obesity and related metabolic disorders.**



Obesity and its comorbidities, including type 2 diabetes, represent a global health threat and a rapidly increasing burden to economic prosperity[1]. Therapeutic intervention is urgently required because lifestyle modification has proven mostly ineffective. Despite this vast unmet need, potent and safe pharmacological options that effectively promote weight loss and improve metabolic health have largely remained elusive[2], partly because many drug interventions historically directed at single molecular targets have exhibited insufficient efficacy or unacceptable safety when used chronically[3]. However, new multimolecular therapies have shown enhanced clinical weight loss[4–6], and single-molecule peptides integrating the complementary actions of multiple endogenous metabolically-related hormones have emerged as one of the more promising clinical candidates for reversing obesity[7–13].

We sought to explore the synergistic metabolic benefits of simultaneous modulation of glucagon, GLP-1 and GIP receptors through a single-molecule hybrid of the three hormones. Glucagon, GLP-1 and GIP are three distinct enteroinsular hormones with unique roles that complement, as well as oppose, each other in the regulation of energy and glucose homeostasis[14–16]. Previously, we reported the ability to assemble balanced, high-potency coagonism for the GLP-1 and glucagon receptors (GLP-1R and GcgR, respectively) into a single peptide[8]. This peptide exhibited a synergistic ability to lower body weight through coordinated thermogenic and anorectic actions, which can be attributed to the glucagon and GLP-1 components, respectively. Simultaneously, we discovered a high-potency, balanced coagonist for the GLP-1R and GIP receptors (GIPR)[9]. This dual incretin coagonist displayed enhanced glycemic efficacy, diminished gastrointestinal toxicity and reduced body weight in preclinical studies, as well as the ability to lower hemoglobin A1C in humans with uncontrolled type 2 diabetes[9]. Having established the unique efficacy of these two coagonists with glucagon and GIP independently complementing GLP-1 by different mechanisms, we hypothesized that, if chemically possible, simultaneous and aligned agonism at all three receptors through a single molecule would produce superior therapeutic outcomes. All three hormones are of comparable size and amino acid composition but sufficiently distinct to provide exquisite potency and specificity

[1]Institute for Diabetes and Obesity, Helmholtz Zentrum München, German Research Center for Environmental Health, Neuherberg, Germany. [2]Department of Medicine, Division of Metabolic Diseases,Technische Universität München, Munich, Germany. [3]Department of Chemistry, Indiana University, Bloomington, Indiana, USA. [4]Marcadia Biotech, Carmel, Indiana, USA. [5]Metabolic Diseases Institute, Division of Endocrinology, Department of Internal Medicine, University of Cincinnati College of Medicine, Cincinnati, Ohio, USA. [6]Research Center, Beijing Hanmi Pharm., Beijing, China. [7]AIT Laboratories, Indianapolis, Indiana, USA. [8]Comprehensive Diabetes Center, Department of Medicine, Division of Endocrinology, Diabetes and Metabolism, University of Alabama at Birmingham, Birmingham, Alabama, USA. [9]Department of Medicine, Lunenfeld Tanenbaum Research Institute, Mt. Sinai Hospital, University of Toronto, Toronto, Ontario, Canada. [10]Pharmaceutical Research and Early Development, Roche Innovation Center Basel, F. Hoffmann-La Roche Ltd., Basel, Switzerland. [11]These authors contributed equally to this work. Correspondence should be addressed to B.F. (brian.finan@helmholtz-muenchen.de), R.D.D. (rdimarch@indiana.edu) or M.H.T. (tschoep@helmholtz-muenchen.de).

Received 24 July; accepted 21 October; published online 8 December 2014; doi:10.1038/nm.3761

for their individual receptors. These similarities render it hypothetically possible to chemically engineer a triple agonist (triagonist) with potent and balanced promiscuity at these three receptors.

Through iterative chemical refinement, we have identified a high-potency, balanced triagonist for GLP-1R, GIPR and GcgR. The triagonist uses distinct amalgamated residues derived from each of the native hormone sequences, which were selected to impart the desired activity profile at each constituent receptor, as well as being optimized for the necessary pharmacokinetics for suitable *in vivo* study. Ultimately, we found that the final iteration of the various triagonists that we tested delivered an apparent and heretofore unparalleled *in vivo* efficacy in reversing diet-induced obesity and type 2 diabetes in rodent models as compared to relevant monoagonists or coagonists.

## RESULTS

### Triple agonism generates synergistic metabolic benefits

We wished to determine whether adiposity and glycemia can be more potently managed through simultaneous agonism at GLP-1R, GIPR and GcgR. Thus, we compared the daily individual treatment of acylated monoagonists at each receptor with the equimolar physical mixture of a previously validated acylated GLP-1R and GIPR (GLP-1/GIP) coagonist[9] with an appropriately matched, acylated GcgR agonist[17] in diet-induced obese (DIO) mice. The GIP analog decreased body weight by 6.4% (**Fig. 1a**) and modestly decreased food intake (**Fig. 1b**). The GLP-1 analog decreased body weight by 12.6% (**Fig. 1a**) and reduced cumulative food intake by more than 50% (**Fig. 1b**). Both GIP and GLP-1 analogs lowered *ad libitum*–fed blood glucose to a similar extent (**Fig. 1c**). The glucagon analog decreased body weight by 11.1% (**Fig. 1a**) but did not affect cumulative food intake (**Fig. 1b**) and increased blood glucose throughout treatment (**Fig. 1c**). The GLP-1/GIP coagonist decreased body weight by 15.4%, outperforming any of the monoagonists in this regard (**Fig. 1a**). This body weight improvement by the coagonist was associated with a lower cumulative food intake relative to that observed with the GLP-1 analog (**Fig. 1b**). Additionally, *ad libitum*–fed blood glucose was decreased to a magnitude similar to that induced by either incretin monoagonist (**Fig. 1c**). Co-administration of the GLP-1/GIP coagonist with an equimolar dose of the glucagon analog decreased body weight by 20.8% (**Fig. 1a**) without further suppression of food intake than that observed with the coagonist alone (**Fig. 1b**). Moreover, simultaneous administration of the GLP-1/GIP coagonist and the GcgR agonist was able to lower blood glucose levels to a point lower than respective single treatments despite the hyperglycemic propensity of the GcgR agonist alone (**Fig. 1c**). These observations served as the foundation to pursue the discovery of unimolecular triagonists simultaneously targeting GLP-1, GIP and glucagon receptors.

### Discovery of a unimolecular, balanced, high-potency GLP-1/GIP/glucagon selective triagonist

The structural and sequence similarities among the three hormones (**Fig. 1d**), coupled with prior structure-function studies[8,9], informed the design of a sequence-hybridized peptide. The challenge was to maintain the individual affinity of each ligand for its receptor and eliminate the structural elements that convey selective preference for each individual receptor, all while maintaining high potency in balanced proportion to each other. Intermediary triagonist candidates were progressively derived from a GLP-1/glucagon coagonist core sequence[8] in an iterative manner to introduce GIP agonism without destroying GLP-1R and GcgR potency. We subsequently tested them for *in vitro* activity at each constituent receptor (**Supplementary Table 1**). All peptide sequences are displayed in **Supplementary Figure 1**, mass spectrometry data are summarized in **Supplementary Table 2**, representative HPLC and liquid chromatography-mass spectrometry data are displayed in **Supplementary Figure 2** and a detailed narrative of triagonist evolution is in the **Supplementary Results**.

Through iterative refinement of the chemical structure, we ultimately succeeded in engineering a highly modified peptide analog that represents the first highly potent, balanced unimolecular triagonist for GLP-1R, GIPR and GcgR. Aminoisobutyric acid was substituted at position 2 to convey resistance to dipeptidyl peptidase IV–mediated degradation and inactivation. We have previously observed that this aminoisobutyric acid substitution also contributes to mixed agonism at GLP-1R and GIPR[9] but is detrimental to glucagon activity. Therefore, we included Glu16, Arg17, Gln20, Leu27 and Asp28 to counteract the negative impact on GcgR potency. These substitutions also serve auxiliary functions to enhance solubility, secondary structure and chemical stability[18]. To enhance time-action and *in vivo* utility, we site-specifically lipidated Lys10 with palmitic acid (C16:0) through a γ-carboxylate spacer. The acyl moiety promotes albumin binding while also supporting mixed agonism[19]. Finally, the triagonist features the C-terminal–extended residues from exendin-4, a reptilian-derived GLP-1 paralog, which results in a single molecule of 39 residues that shows superior solubility, potency and balance at each of the three receptors (**Fig. 1e–g** and **Supplementary Table 1**). Although the triagonist was designed specifically to possess the requisite activity at human receptors, it has a similar activity profile (based on cyclic AMP (cAMP) induction) across all three constituent receptors originating from mice, rats and cynomolgus monkeys (**Supplementary Table 3**). Therefore, the triagonist is suitable for *in vivo* pharmacological and characterization studies across different species in preclinical studies.

As we were able to introduce balanced agonism for three different receptor targets within a single molecule, we surmised that the peptide may bind to additional receptor targets. Therefore, we screened the triagonist at over 70 different receptor targets in high-throughput competitive binding assays. Using strict criteria for a positive result (10% inhibition of native ligand binding), we show that the triagonist displayed no cross-reactive binding to any of the other screened receptors (**Supplementary Table 4**). Notably, the triagonist did not bind to the vasoactive intestinal peptide receptor or the pituitary adenylate cyclase–activating polypeptide receptor, two members of the glucagon/secretin class of peptide hormones. Therefore, we concluded that the triagonist is highly specific for GLP-1R, GIPR and GcgR.

### The unimolecular triagonist possesses *in vitro* and *in vivo* activity attributed to each targeted receptor

To explore whether the triagonist possesses *in vitro* activity at each constituent receptor, we investigated the effects on cAMP accumulation in cell lines that represent conventional target tissues of GLP-1, GIP and glucagon. In a mouse pancreatic beta cell line (MIN6) that abundantly expresses GLP-1R, the GLP-1/GIP coagonist and the triagonist induced cAMP production with potency similar to that of native GLP-1 (**Supplementary Table 5**), confirming full GLP-1R activity at pancreatic beta cells. In differentiated 3T3-L1 mouse adipocytes, which abundantly express GIPR[20], cAMP production was induced by GIP, the GLP-1/GIP coagonist and the triagonist with comparable potency (**Supplementary Table 5**), confirming full GIPR activity at adipocytes. In rat hepatocytes, which endogenously express GcgR[21], cAMP production was induced by glucagon and the triagonist with similar potency, whereas the GLP-1/GIP coagonist demonstrated 30-fold less potency (**Supplementary Table 5**), thus confirming full GcgR activity at hepatocytes.

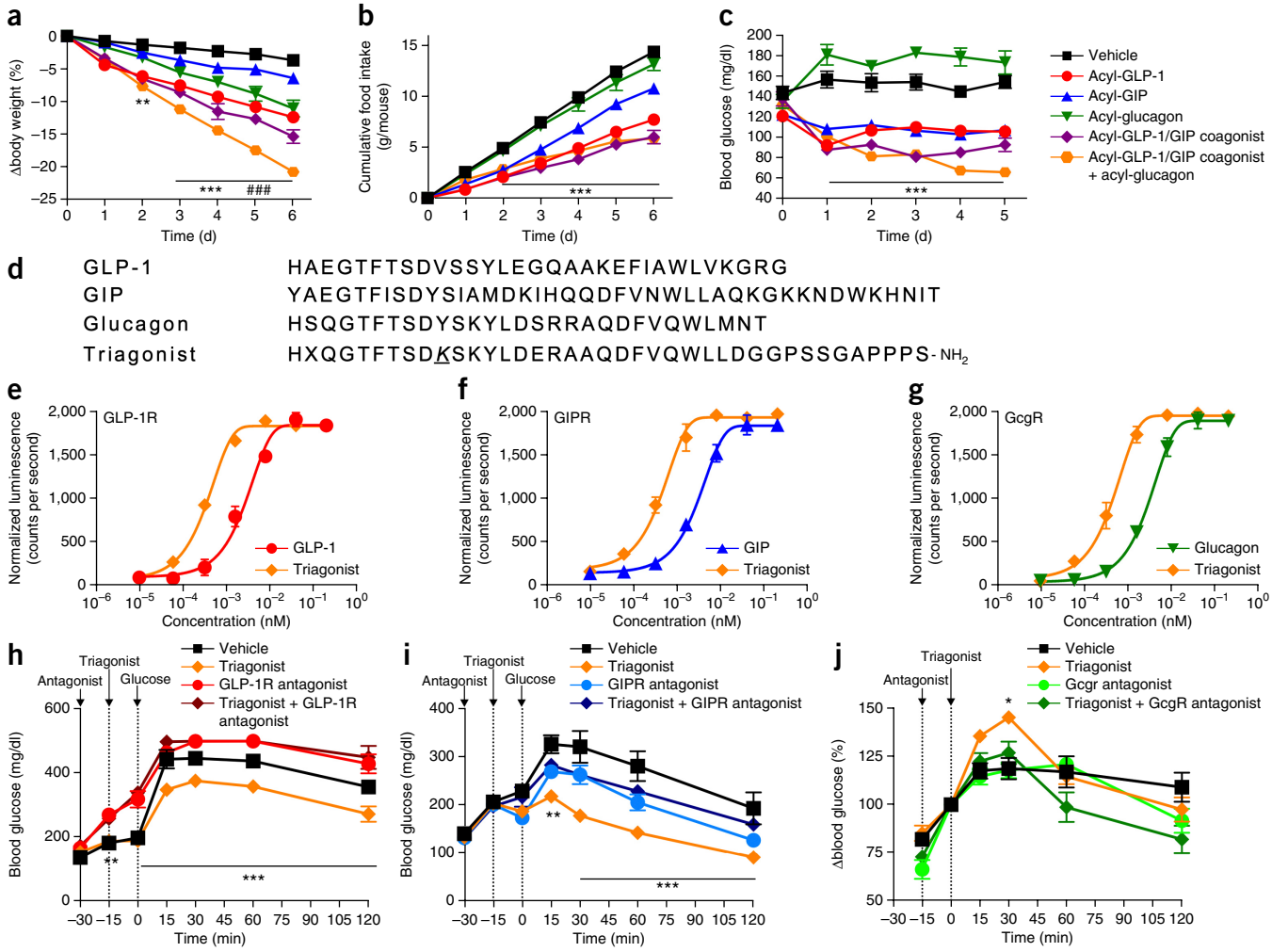


**Figure 1** *In vivo* demonstration of GLP-1, GIP and glucagon triple agonism through coadministration and unimolecular peptides. (**a**–**c**) Effects on body weight change (**a**), cumulative food intake (**b**) and *ad libitum* fed blood glucose (**c**) of male DIO mice (age 9 months; $n = 8$ per group) treated with acylated analogs of GLP-1, GIP, dual incretin coagonist, glucagon or the equimolar coadministration of the dual incretin coagonist with the glucagon analog; all at a dose of 10 nmol per kg body weight (nmol $kg^{-1}$). (**d**) Sequences of native GLP-1, GIP and glucagon compared with the GLP-1/GIP/glucagon triagonist. Aminoisobutyric acid is denoted as X. Lysine with a γE-$C_{16}$ acyl attached through the side chain amine is denoted as *K*. (**e**–**g**) Representative dose-response curves for activation of the native hormone and the triagonist at the human GLP-1R (**e**), GIPR (**f**) and GcgR (**g**). Data in (**e**–**g**) is the normalized response from three independent experiemnts. (**h**) Acute effects on intraperitoneal glucose tolerance in male DIO mice (age 12 months; $n = 8$ per group) treated with vehicle, the triagonist (1 nmol $kg^{-1}$) or a GLP-1R antagonist (1 μmol $kg^{-1}$), or pretreated with the GLP-1R antagonist before the triagonist. (**i**) Acute effects on intraperitoneal glucose tolerance in male *Glp1r*$^{-/-}$ DIO mice (age 12 months; $n = 8$ per group) treated with vehicle, the triagonist (2 nmol $kg^{-1}$) or a GIPR antagonist (2 μmol $kg^{-1}$), or pretreated with the GIPR antagonist before the triagonist. (**j**) Acute effects on glycemia in male STZ mice (age 13 months; $n = 8$ per group) treated with vehicle, the triagonist (1 nmol $kg^{-1}$) or a GcgR antagonist (1 μmol $kg^{-1}$) or pretreated with the GcgR antagonist before the triagonist. Data in **a**–**j** represent mean ± s.e.m. $^{*}P < 0.05$, $^{**}P < 0.01$, $^{***}P < 0.001$, determined by regular one- or two-way analysis of variance (ANOVA) comparing vehicle with compound injections, and $^{\#\#\#}P < 0.001$, as determined by ANOVA comparing the dual incretin coagonist with its coadministration with the glucagon analog. In both comparisons, ANOVA was followed by Tukey *post hoc* multiple comparison analysis to determine statistical significance.

To investigate whether the triagonist possesses *in vivo* activity at each cognate receptor, we compared the acute glycemic effects using selective antagonists at each receptor in different rodent models. To confirm the presence of GLP-1 activity, we administered the triagonist to DIO mice pretreated with a validated GLP-1R antagonist[22]. Pretreatment with the GLP-1R antagonist ameliorated the improved glucose tolerance observed with the triagonist alone (**Fig. 1h**), thus confirming *in vivo* GLP-1 activity. To confirm the presence of GIP activity, we administered the triagonist to DIO *Glp1r*$^{-/-}$ mice pretreated with a validated GIPR antagonist[9]. Similarly, pretreatment with the GIPR antagonist blunted the improvement observed with the triagonist alone (**Fig. 1i**), thus demonstrating *in vivo* GIP activity.

To confirm the presence of GcgR activity *in vivo*, we administered the triagonist to streptozotocin-treated mice pretreated with a GcgR antagonist and assessed induced hyperglycemia brought on by the glucagon component of the peptide. Pretreatment with the GcgR antagonist inhibited the acute, transient hyperglycemic effect otherwise observed with the triagonist alone (**Fig. 1j**), which shows that the triagonist possesses classical *in vivo* GcgR activity.

## Metabolic benefits of the triagonist are superior to those of the respective dual agonists

To confirm that the triagonist delivers enhanced metabolic improvement indicative of *in vivo* triple agonism, we compared chronic daily

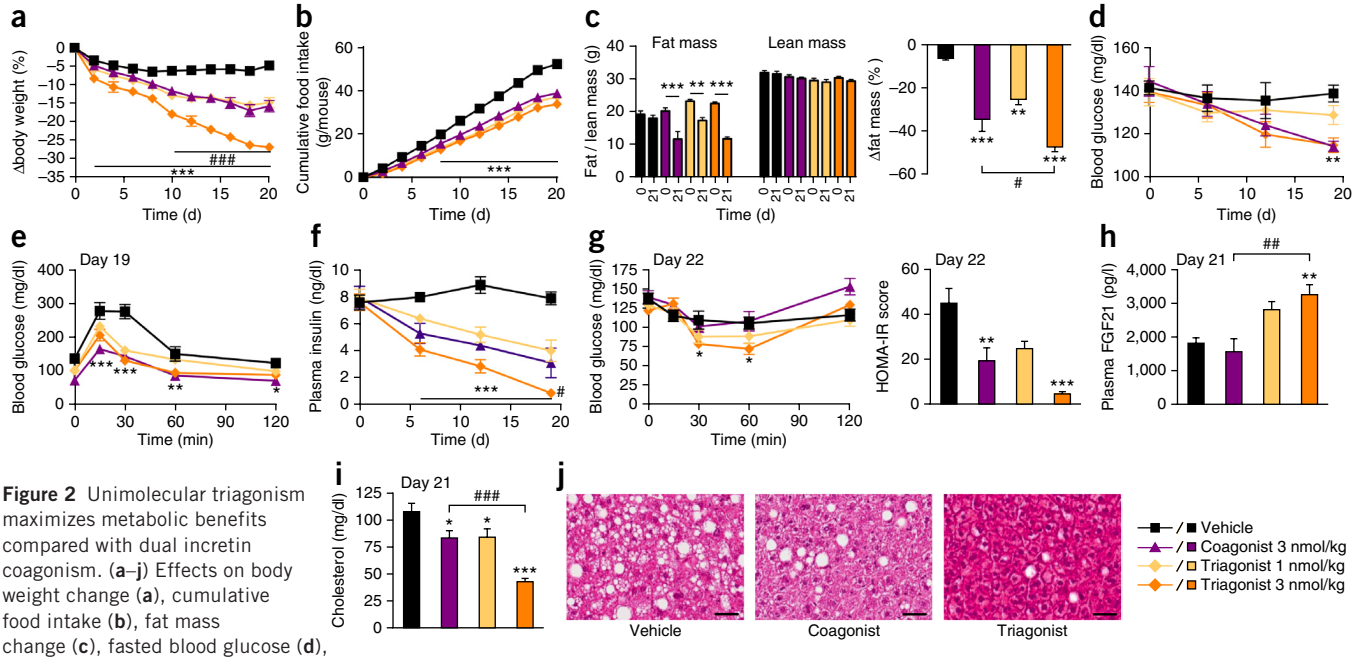


**Figure 2** Unimolecular triagonism maximizes metabolic benefits compared with dual incretin coagonism. (**a**–**j**) Effects on body weight change (**a**), cumulative food intake (**b**), fat mass change (**c**), fasted blood glucose (**d**), intraperitoneal glucose tolerance (**e**), plasma insulin (**f**), insulin tolerance and Homeostasis Model Assessment of insulin resistance (HOMA-IR) score (**g**), plasma FGF21 (**h**), and plasma cholesterol (**i**) of male DIO mice (age 7 months; $n = 8$ per group) treated daily with vehicle, a dual incretin coagonist (3 nmol kg$^{-1}$), or the GLP-1/GIP/glucagon triagonist at 1 nmol kg$^{-1}$ or 3 nmol kg$^{-1}$. (**j**) Effects on hepatocellular vacuolation after the 21 d of treatment with vehicle, the dual incretin coagonist (3 nmol kg$^{-1}$), or the triagonist (3 nmol kg$^{-1}$). Scale bars in **j**, 50 µm. Data in **a**–**i** represent mean ± s.e.m. $^{*}P < 0.05$, $^{**}P < 0.01$, $^{***}P < 0.001$, determined by one- or two-way ANOVA comparing vehicle with compound injections. $^{\#}P < 0.05$, $^{\#\#}P < 0.01$, $^{\#\#\#}P < 0.001$, determined by ANOVA comparing dual incretin coagonist with triagonist injections. In both comparisons, ANOVA was followed by Tukey *post hoc* multiple comparison analysis to determine statistical significance. Images in **j** are representative of 3 samples from 8 mice per treatment group.

treatment with the triagonist to treatment with the three structurally related and pharmacokinetically matched coagonists. As a first evaluation, we compared the triagonist with an equimolar dose of a GLP-1/glucagon coagonist and a GIP/glucagon coagonist in DIO mice, with liraglutide (a lipidated GLP-1 analog) included as a benchmark comparator. At this low dose, liraglutide and the GIP/glucagon coagonist did not improve body weight or glucose tolerance compared to vehicle in DIO mice, whereas the GLP-1/glucagon coagonist lowered body weight by 9.9% (**Supplementary Fig. 3a**). This body weight loss occurred without a concomitant improvement in intraperitoneal glucose tolerance (**Supplementary Fig. 3b**,**c**). Treatment with the triagonist lowered body weight by 15.1%, a substantial potentiation compared with liraglutide and both GIP/glucagon and GLP-1/glucagon coagonists. The triagonist was the only compound to markedly improve glucose tolerance (**Supplementary Fig. 3b**) and reduce food intake (**Supplementary Fig. 3d**) at this low dose. Notably, we were able to induce a similar effect on body weight loss with the triagonist as in our previous report of GLP-1/glucagon co-agonism[8], but at nearly one-twentieth of the dose. We believe the glucagon component within the triagonist contributes substantial weight-lowering efficacy that can potentiate that of the dual incretin action. Thus, we extensively compared the metabolic efficacy of the triagonist with that of the validated GLP-1/GIP coagonist[9] in subsequent studies.

We compared the triagonist with a GLP-1/GIP coagonist of matched potency at equivalent doses in DIO mice. The coagonist decreased body weight by 15.7%, whereas the triagonist decreased body weight by 26.6% after 20 d (**Fig. 2a**). The triagonist decreased body weight in a dose-dependent manner, such that a 33% lower dose of the triagonist decreased body weight by 14.7%, which is comparable to the coagonist at a threefold higher dose. Both mixed agonists caused a similar reduction in food intake (**Fig. 2b**) without influencing gastric emptying (**Supplementary Fig. 4a**). Such treatment generates the loss of fat mass without altering lean mass (**Fig. 2c**). The coagonist and the triagonist were equally effective in lowering *ad libitum*–fed blood glucose (**Fig. 2d**) and improving glucose tolerance (**Fig. 2e**) without inducing hypoglycemia (**Supplementary Fig. 4b**), demonstrating that chronic GcgR agonism does not diminish the sizable glycemic improvement achieved by simultaneous dual incretin receptor coagonism. However, the triagonist lowered circulating concentrations of insulin to a greater extent than that achieved with the coagonist (**Fig. 2f**), which is indicative of improved insulin sensitivity, reflected by an improved insulin tolerance and lower Homeostasis Model Assessment of insulin resistance score (**Fig. 2g**). The triagonist, but not the coagonist, increased plasma concentrations of fibroblast growth factor 21 (FGF21; **Fig. 2h**), which is a selective action of the glucagon component within the triagonist. Furthermore, the triagonist lowered the plasma concentration of cholesterol to a greater extent than the coagonist (**Fig. 2i**). Evaluations of other clinical chemical markers did not reveal any substantial differences between the treatments (**Supplementary Fig. 4c**–**l**). The triagonist had a pronounced effect on lowering hepatic lipid content and hepatocellular vacuolation (**Fig. 2j**). Collectively, these results demonstrate that greater metabolic efficacy can be gained by treatment with a unimolecular GLP-1R, GIPR and GcgR triagonist than with a dual incretin coagonist. A similar effect on body weight loss can be achieved with the triagonist as in our previous reports of co-agonism, but at a much lower dose of the triagonist.

We can exclude that prolonged duration of action is contributing to the enhanced efficacy of the triagonist compared with the GLP-1/GIP coagonist because the pharmacokinetic parameters across different

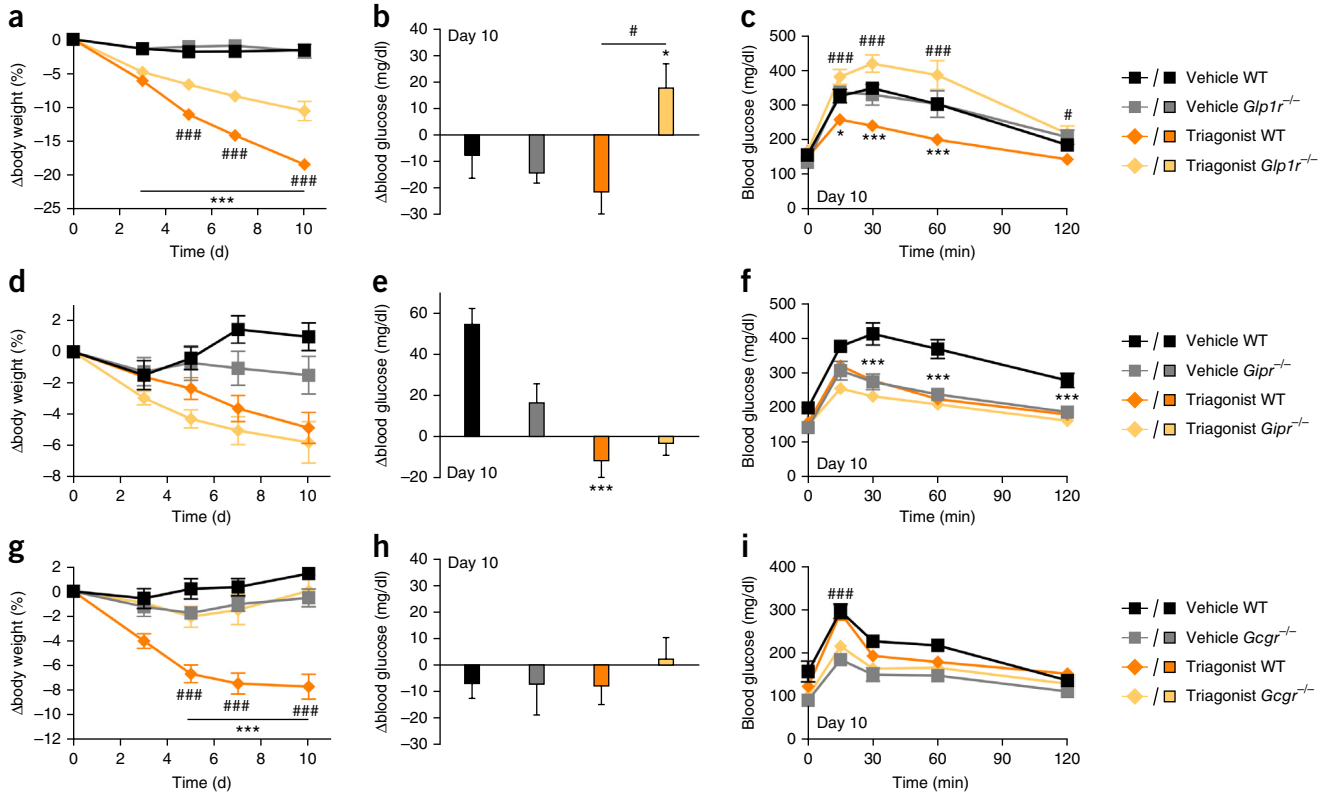


**Figure 3** The metabolic and glycemic benefits of the triagonist are blunted in *Glp1r*$^{-/-}$, *Gipr*$^{-/-}$ and *Gcgr*$^{-/-}$ mice. (**a**–**c**) Effects on body weight change (**a**), fasted blood glucose change (**b**) and intraperitoneal glucose tolerance (**c**) in wild-type (WT) or *Glp1r*$^{-/-}$ male HFD mice (age 7 months; $n = 8$ per group for each genotype). (**d**–**f**) Effects on body weight change (**d**), fasted blood glucose change (**e**) and (intraperitoneal glucose tolerance (**f**) in male wild-type ($n = 6$ per group) or *Gipr*$^{-/-}$ ($n = 7$ per group) HFD mice (age 5 months). (**g**–**i**) Effects on body weight change (**g**), fasted blood glucose change (**h**) and intraperitoneal glucose tolerance (**i**) in male wild-type ($n = 5$) or *Gcgr*$^{-/-}$ ($n = 7$) HFD mice. All mice were treated with vehicle or the triagonist via subcutaneous injections administered every other day at a dose of 10 nmol kg$^{-1}$. Data in **a**–**i** represent mean ± s.e.m. $^{*}P < 0.05$, $^{***}P < 0.001$, determined by ANOVA comparing vehicle with compound injections within each genotype. $^{\#}P < 0.05$, $^{\#\#\#}P < 0.001$, determined ANOVA comparing treatment of the triagonist between genotypes. In both comparisons, ANOVA was followed by Tukey *post hoc* multiple comparison analysis to determine statistical significance.

species are similar between the two peptides. The average half-life of the triagonist following a bolus subcutaneous dose is approximately 5 h in rodents (**Supplementary Table 6**), which is similar to the reported half-life of 4–8 h for liraglutide in rodents[23].

As a point of reference, we compared the *in vitro* activity of this triagonist with two recently reported peptides with purported triple agonism[24,25]. Both of these reported peptides (termed YAG-glucagon[24] and [$_{D}$A$^{2}$]GLP-1/GcG (ref. 25)) demonstrate nearly one-thousandth the activity at least at one of the three receptors compared with the native hormones (**Supplementary Table 1**). Additionally, these peptides were massively imbalanced in activity, rendering them at best extremely low-potency coagonists and certainly not triagonists. In DIO mice, twice-daily administration of these compounds at a cumulative dose of 50 nmol kg$^{-1}$ d$^{-1}$, which is a dose 16 times higher than that of our triagonist, failed to reduce body weight, food intake or blood glucose or improve glucose tolerance compared with vehicle treatment, whereas exendin-4 improved all the aforementioned parameters (**Supplementary Fig. 5a–d**). These *in vivo* results confirm the imbalanced activity and reduced receptor potency of the purported triagonists and demonstrate that these peptides are substantially inferior in terms of metabolic efficacy, even compared with the classical GLP-1R monoagonist exendin-4. Accordingly, these peptides fail as potent mixed agonists; therefore, they do not qualify as triagonists and should be used with caution.

### Chronic treatment with the triagonist safely lowers body weight without hypoglycemic risk

Although we did not observe hypoglycemia or a substantial loss of lean mass after chronic treatment in DIO mice, we were still concerned about the safety of the considerable glucose-lowering and weight-lowering efficacy. The triagonist induced a dose-dependent decrease in blood glucose following a single-bolus intraperitoneal injection in lean, euglycemic mice (**Supplementary Fig. 6a**). Notably, we did not observe hypoglycemia at any of the doses tested when monitored 24 h after injection. Additionally, the triagonist did not reduce body weight, lean mass, or food intake (**Supplementary Fig. 6b–d**) after chronic treatment at any of the doses tested in these lean mice.

To test whether the triagonist has sustained efficacy in a longer-term setting, we treated DIO rats for 11 weeks with two doses of the triagonist. By 11 weeks, the lower dose of the triagonist decreased body weight by 9.7% and the higher dose decreased body weight by 26.4% (**Supplementary Fig. 6e**), along with dose-dependent reductions in food intake (**Supplementary Fig. 6f**). This superior body weight loss induced by the triagonist may limit the dose escalation in translational and toxicological studies. However, 2-week follow-up analysis in DIO mice that received the triagonist for 3 weeks revealed that the mice regained body weight to near baseline levels, and mild hyperglycemia was recovered (**Supplementary Fig. 6g,h**), which indicates that the triagonist did not cause irreversible damage in these preclinical studies.

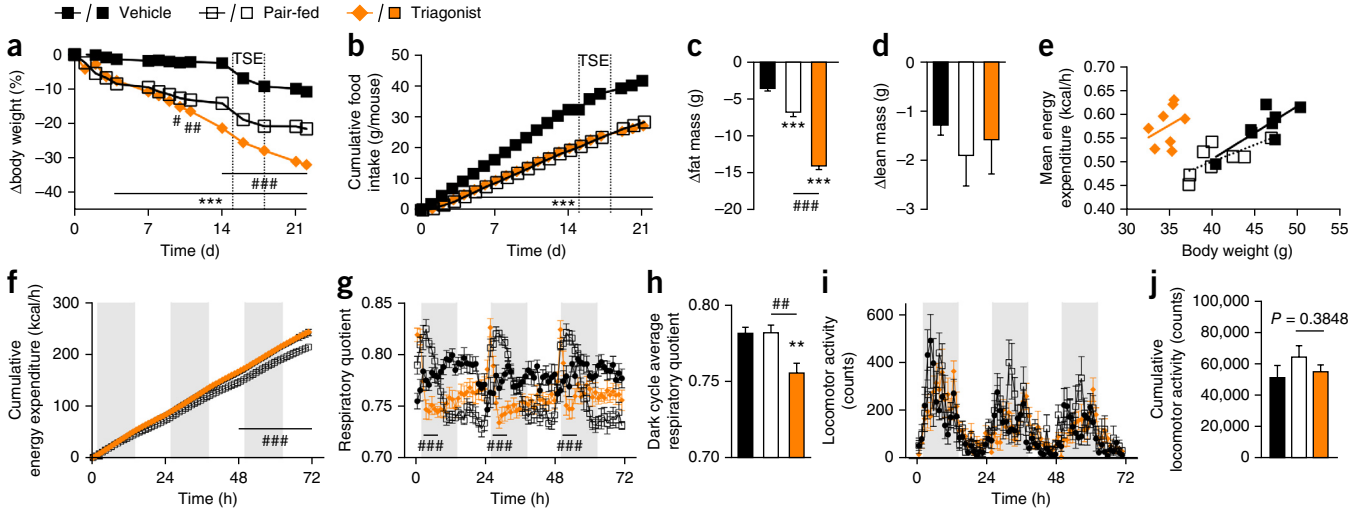


**Figure 4** Addition of glucagon activity contributes thermogenic character to the triagonist. (**a**–**j**) Effects on body weight change (**a**), cumulative food intake (**b**), fat mass change (**c**), lean mass change (**d**), body weight–correlated average energy expenditure (**e**), cumulative energy expenditure (**f**), real-time respiratory quotient (**g**), average respiratory quotient measured during the dark cycle (**h**) and real-time (**i**) and cumulative (**j**) locomotor activity of male DIO mice (age 6 months; $n = 8$ per group) treated daily with vehicle or GLP-1/GIP/glucagon triagonist (2 nmol kg$^{-1}$), or control mice pair-fed with triagonist-treated mice. Dotted lines in **a** and **b** represent times for indirect calorimetry analysis, and shaded regions in **f**, **g**, and **i** represent time during the dark cycle of light. Data in **a**–**j** represent mean ± s.e.m. $^{**}P < 0.01$, $^{***}P < 0.001$, determined by ANOVA comparing vehicle with test group injections. $^{\#}P < 0.05$, $^{\#\#}P < 0.01$, $^{\#\#\#}P < 0.001$, determined by ANOVA followed by Tukey *post hoc* multiple comparison analysis comparing pair-fed controls to triagonist injections. In **a**, the time during which indirect calorimetry was assessed is indicated by the vertical dashed line and the TSE label, which is the system of metabolic cages used to measure indirect calorimetry.

### Improved metabolic and glycemic benefits of triple agonism depend on GLP-1R and GIPR signaling

We studied the contribution of the GLP-1 component of the triagonist by testing its metabolic efficacy in high-fat diet–fed (HFD) *Glp1r*$^{-/-}$ mice. The triagonist decreased body weight by 18.3% in wild-type HFD mice, yet by only 10.5% in HFD *Glp1r*$^{-/-}$ mice (**Fig. 3a**). This diminished efficacy was also reflected in fat mass change and cumulative food intake (**Supplementary Fig. 7a**,**b**). Without GLP-1 activity to enhance GIP activity in counteracting the hyperglycemic character of GcgR agonism, the triagonist increased blood glucose in HFD *Glp1r*$^{-/-}$ mice, a trait noticeably absent from wild-type HFD controls (**Fig. 3b**). Mirroring this, the triagonist improved glucose tolerance in wild-type mice but not in *Glp1r*$^{-/-}$ mice, in which it in fact worsened glucose tolerance (**Fig. 3c**). These results demonstrate the contribution of GLP-1 activity to the full efficacy of the triagonist and underscore the necessity of integrated GLP-1 activity to minimize the diabetogenic risk of chronic and maximal GcgR agonism.

We explored the contribution of the GIP component of the triagonist by testing its metabolic efficacy in HFD *Gipr*$^{-/-}$ mice. Unlike in HFD *Glp1r*$^{-/-}$ mice, the triagonist induced comparable reductions in body weight (**Fig. 3d**), fat mass and food intake (**Supplementary Fig. 7c**,**d**) in both HFD wild-type and HFD *Gipr*$^{-/-}$ mice. Similar to the case in HFD *Glp1r*$^{-/-}$ mice, the glucose-lowering effect of the triagonist was lost in HFD *Gipr*$^{-/-}$ mice (**Fig. 3e**), but the remaining GLP-1 activity was able to prevent the rise in blood glucose that we observed in HFD *Glp1r*$^{-/-}$ mice. This result shows that integrated GIP activity within the triagonist contributes to the glucose-lowering effect and helps buffer against the hyperglycemic effect of glucagon activity, albeit to a lesser degree than GLP-1. This was also evident in glucose tolerance, where the beneficial effect of triagonist was muted in HFD *Gipr*$^{-/-}$ mice (**Fig. 3f**). However, it cannot be entirely excluded that the loss of the glycemic benefits and lack of the weight-lowering effect of the triagonist in *Gipr*$^{-/-}$ mice was in part due to their inherent resistance to HFD-induced glucose intolerance[26].

### Improved energy metabolism benefits of tri-agonism depend on GcgR signaling

We studied the contribution of the glucagon component of the triagonist by testing its metabolic efficacy in *Gcgr*$^{-/-}$ mice fed a HFD. The weight-lowering efficacy of the triagonist was lost in a low-dose treatment of these HFD *Gcgr*$^{-/-}$ mice compared with HFD wild-type controls. The triagonist decreased body weight by 7.7% (**Fig. 3g**) and lowered fat mass in wild-type mice (**Supplementary Fig. 7e**), yet had no measurable effect on body weight loss in HFD *Gcgr*$^{-/-}$ mice (**Fig. 3g**). Likewise, the triagonist lost its anorectic efficacy (**Supplementary Fig. 7f**) and lowering effect on fasted blood glucose (**Fig. 3h**), and failed to improve glucose tolerance in these HFD *Gcgr*$^{-/-}$ (**Fig. 3i**), which may be partially attributed to the existing hypoglycemia and inherent protection from glucose intolerance of *Gcgr*$^{-/-}$ mice[27].

We have previously demonstrated that changes in energy expenditure are not a key contributor to the weight-lowering efficacy of the GLP-1/GIP coagonist[9] but do contribute to the efficacy of the GLP-1/glucagon coagonist, which is attributed to the integrated glucagon pharmacology[8]. Supporting this, we did not observe any difference in food intake between wild-type mice treated with the dual incretin coagonist and those treated with the triagonist despite substantial differences in weight loss, thus supporting that energy expenditure mechanisms contribute to the overall efficacy. Therefore in DIO mice, we compared the metabolic efficacy of the triagonist to that of pair-fed controls. The triagonist caused a greater reduction in body weight (32.0%) compared to that observed in pair-fed controls (21.6%; **Fig. 4a**,**b**), which is the result of loss of fat mass, not lean mass (**Fig. 4c**,**d**). After body weight segregation, we observed significantly enhanced energy expenditure in triagonist-treated DIO mice compared with the pair-fed controls (**Fig. 4e**,**f**; $P < 0.001$). When

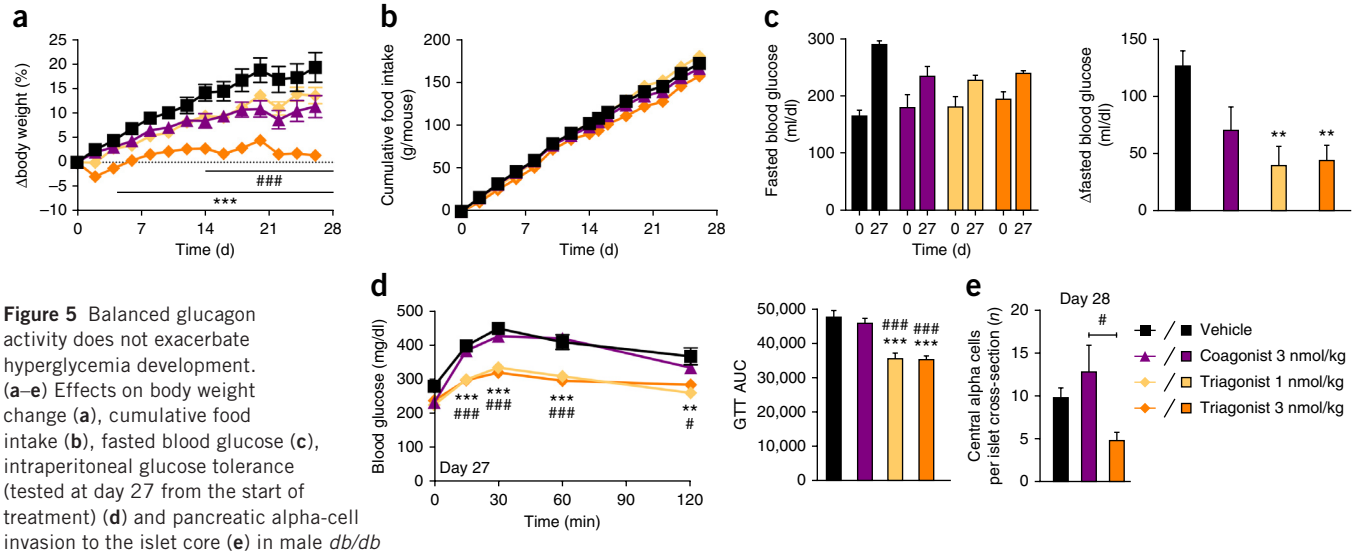


**Figure 5** Balanced glucagon activity does not exacerbate hyperglycemia development. (**a**–**e**) Effects on body weight change (**a**), cumulative food intake (**b**), fasted blood glucose (**c**), intraperitoneal glucose tolerance (tested at day 27 from the start of treatment) (**d**) and pancreatic alpha-cell invasion to the islet core (**e**) in male *db/db* mice ($n = 8$ per group) treated daily, starting at 9 weeks of age, with vehicle, a dual incretin coagonist (3 nmol $kg^{-1}$), or the GLP-1/GIP/glucagon triagonist at 1 nmol $kg^{-1}$ or 3 nmol $kg^{-1}$ (tested at day 28 from the start of treatment). Data in **a**–**e** represent mean ± s.e.m. $^{**}P < 0.01$, $^{***}P < 0.001$, determined by ANOVA comparing vehicle with the highest dose of triagonist injections. $^{\#}P < 0.05$, $^{\#\#\#}P < 0.001$, determined by ANOVA comparing coagonist with triagonist injections at equimolar doses. In both comparisons, ANOVA was followed by Tukey *post hoc* multiple comparison analysis to determine statistical significance. Statistical comparison of data in the left panel of **d** was determined by two-way ANOVA followed by Tukey *post hoc* multiple comparison analysis comparing triagonist injections with pair-fed controls over time. GTT, glucose tolerance test; AUC, area under the concentration time curve.

compared with both *ad libitum*–fed and pair-fed controls, triagonist-treated mice had a significantly lower respiratory quotient during times of feeding (**Fig. 4g**,**h**; $P < 0.01$) without any change in locomotor activity (**Fig. 4i**,**j**), suggesting altered nutrient partitioning to greater fat oxidation. Collectively, the data demonstrate that the weight-lowering efficacy of the triagonist is not simply a consequence of reduced caloric intake.

## GcgR signaling component of the triagonist does not exacerbate preexisting hyperglycemia

We explored whether the enhanced metabolic efficacy of the triagonist observed in insulin-resistant obese mice would translate to rodent models of type 2 diabetes. We used *db/db* mice at 6 weeks of age, immediately before the development of hyperglycemia, and assessed the capacity of the triagonist to prevent the development of spontaneous diabetes compared with the dual incretin coagonist. The triagonist prevented the excessive weight gain observed in vehicle-treated mice and showed improvement over the effect observed with the coagonist (**Fig. 5a**). Despite these differences, cumulative food intake was not altered with either treatment (**Fig. 5b**). Furthermore, the triagonist protected *db/db* mice from fasted hyperglycemia at both doses tested, an effect comparable to that of the GLP-1/GIP coagonist (**Fig. 5c**). In fact, the triagonist was superior compared with the coagonist in lessening glucose intolerance (**Fig. 5d**) and preserving proper islet architecture, as assessed by reduced alpha cell infiltration within the core of pancreatic islets (**Fig. 5e**) after 4 weeks of treatment.

We next assessed the effects of the triagonist in Zucker diabetic fatty (ZDF) rats. In a dose-dependent manner, the triagonist improved body weight and fasting blood glucose with a rapid onset and sustained efficacy (**Supplementary Fig. 8a**,**b**), improved glucose tolerance and hemoglobin A1C, and preserved proper islet cytoarchitecture compared with vehicle control (**Supplementary Fig. 8c**–**e**). Notably, these glycemic improvements were maintained in the high-dose group 3 weeks after treatment cessation (**Supplementary Fig. 8d**,**e**), despite body weight regain back to a level comparable to that of vehicle-treated controls (**Supplementary Fig. 8f**), demonstrating an ability to ameliorate diabetes progression in rodent models of spontaneous diabetes.

## Optimal metabolic benefits of triple agonism predominantly depend on fine-tuning the glucagon component

We explored the relative degree of glucagon activity necessary to maintain the maximal weight-lowering efficacy of a triagonist. We assembled a series of peptides selectively laddered in their relative GcgR agonism through modification at the third amino acid, as we observed that GLP-1 and GIP were relatively insensitive to changes at this position (**Supplementary Table 1**, peptides 21–27). Notably, substitution with methionine sulfoxide ($Met(O)^3$) resulted in an analog with 5% of initial glucagon character, and glutamic acid substitution ($Glu^3$) resulted in negligible glucagon activity (**Supplementary Table 1**, peptides 26–27). In DIO mice, the balanced triagonist decreased body weight by 22.8% and the sequence-matched coagonist reduced body weight by 14.9%, reemphasizing the relative importance of the integrated and balanced GcgR agonism to the weight-lowering efficacy. The $Met(O)^3$ analog (imbalanced triagonist) decreased body weight by 19.3% (**Fig. 6a**), which is intermediate compared to the weight loss induced by the triagonist and GLP-1/GIP coagonist. However, this imbalanced triagonist had a more pronounced effect on lowering *ad libitum*–fed blood glucose than the balanced triagonist, resulting in enhanced glucose lowering analogous to that achieved with the GLP-1/GIP coagonist (**Fig. 6b**).

To more deeply determine the relative beneficial limits and risk associated with excessive glucagon pharmacology in DIO mice, we supplemented a constant low dose of the dual incretin coagonist[9] with escalating doses of the acyl-glucagon agonist. The acylated glucagon analog alone displayed a dose-dependent and robust weight-lowering efficacy, which was appreciably enhanced when the dual-incretin coagonist was co-administered at a constant low dose (**Fig. 6c**).

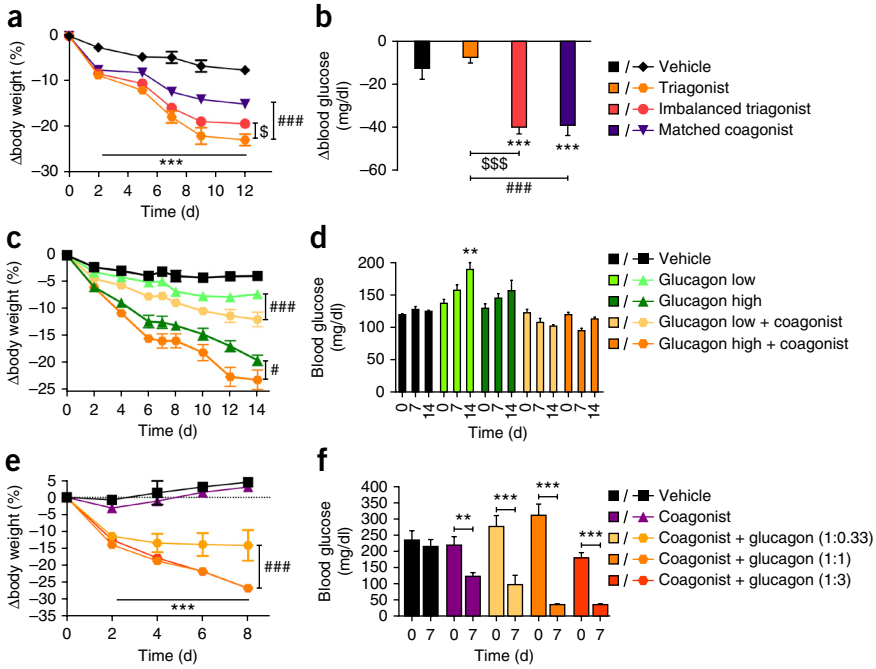


**Figure 6** Fine-tuning of glucagon activity within the triagonist alters metabolic and glycemic efficacies. (**a**,**b**) Effects on body weight change (**a**) and fasted blood glucose change (**b**) in male DIO mice (age 6 months; $n = 8$ per group) treated with vehicle, the balanced triagonist, an imbalanced triagonist with 5% glucagon activity or a dual incretin coagonist. Mice in **a**,**b** were treated with respective compounds at a dose of 10 nmol $kg^{-1}$ administered every other day. (**c**,**d**) Effects on body weight change (**c**) and fasted blood glucose (**d**) in male DIO mice (age 8 months; $n = 8$ per group) treated daily with vehicle, escalating doses (3 or 10 nmol $kg^{-1}$) of an acylated glucagon analog or escalating doses of the acylated glucagon analog co-administered with a low dose (1 nmol $kg^{-1}$) of the dual incretin coagonist. (**e**,**f**) Effects on body weight change (**e**) and fasted blood glucose (**f**) in 9-week-old *db/db* mice ($n = 8$ per group) treated daily with vehicle, the dual incretin coagonist at a dose of 10 nmol $kg^{-1}$ or the dual incretin coagonist with escalating doses of the acylated glucagon analog, depicted as equivalent molar ratio to the coagonist. Data in **a**–**f** represent mean ± s.e.m. $^{**}P < 0.01$, $^{***}P < 0.001$, determined by ANOVA comparing vehicle with triagonist injections. $^{\#}P < 0.05$, $^{\#\#}P < 0.01$, $^{\#\#\#}P < 0.001$, determined by ANOVA comparing coagonist with triagonist injections. $^{\$}P < 0.05$, $^{\$\$\$}P < 0.001$ determined by ANOVA comparing triagonist with imbalanced triagonist injections. In all comparisons, ANOVA was followed by Tukey *post hoc* multiple comparison analysis to determine statistical significance.

The maximal dose of the glucagon analog alone increased blood glucose, but this rise was prevented when supplemented with the dual incretin coagonist, even at a relative ratio as little as one-third to one-tenth of the glucagon dose (**Fig. 6d**).

Finally, we challenged diabetic *db/db* mice with more extreme glucagon dosing to test the capacity of dual incretin coagonism to prevent the glucagon-mediated rise in blood glucose. We co-administered escalating doses of the acylated glucagon analog with a low dose of the GLP-1/GIP coagonist. This physical mixture resulted in a dose-dependent potentiation of body weight loss, with a maximal effect using a 1:1 molar ratio (**Fig. 6e**). Even a threefold molar excess of the glucagon analog failed to increase blood glucose in these *db/db* mice treated simultaneously with the dual incretin coagonist (**Fig. 6f**). Collectively, these observations demonstrate that the dual incretin components counterbalance the potential diabetogenic liability of excessive GcgR agonism, which is something that seemed more fragile when using just GLP-1 to buffer glucagon action[8,10,28].

## DISCUSSION

Here we explored the chemical capability of combining agonism at the glucagon, GLP-1 and GIP receptors into a single molecule, as well as the synergistic efficacy of this concerted triple agonism to reverse perturbed metabolism in rodent models of obesity and diabetes. As a first-degree proof of principle, we simulated *in vivo* triple agonism by *in situ* co-administration of a glucagon analog as a second molecule with the validated GLP-1/GIP coagonist. This adjunctive triple agonism amplified the metabolic efficacy of the dual incretin in obese mice, thus establishing the pharmacological foundation to pursue the uncertain creation of a unimolecular triagonist with glucagon, GLP-1 and GIP activities.

The design of the triagonist was inspired by our previous observations in the discovery process of the mixed coagonists, as well as by the established sequence differences among the three endogenous hormones. The goal was to maintain high activity across all three receptors yet eliminate the inherent high selectivity resident in the native hormones. The core 29-residue GLP-1/glucagon coagonist peptide[8] proved resistant to our best efforts to identify a change that would introduce GIP activity. The breakthrough was the addition of the exendin-4-based C-terminal extended sequence to a lipidated, dipeptidyl peptidase IV–protected intermediate analog. This elongation provided a triagonist of equal balance at all three receptors with superior potency relative to the native hormones. Notably, this single-peptide triagonist is a hybridized peptide, not simply a conjugate multimer of the native ligands, and it features a single receptor-binding face. This conveys concerted yet independent and promiscuous agonism at each constituent receptor without cross-reactivity at other related G protein–coupled receptors, essentially serving as a master key to unlock signaling at each individual receptor.

We demonstrate here that this unimolecular triagonist potently reverses diet-induced obesity and prevents diabetes progression in rodent models to a greater extent than reciprocal coagonism at the individual receptors. We were able to induce a comparable effect size with the triagonist, in terms of weight loss and glycemic control, as we independently reported with GLP-1/glucagon[8] and GLP-1/GIP[9] coagonists, but at substantially lower doses, which cannot be attributed to differences in pharmacokinetics. We demonstrated that concerted triple agonism exceeds dual incretin coagonism in terms of improving body weight and composition. This is partially attributed to the supplementation of glucagon pharmacology and its subsequent contribution to enhancing energy expenditure and hepatic lipid handling, some of which may be enabled by glucagon-mediated FGF21 induction[17], which is only observed with the triagonist. We believe that triple agonism represents a sizable step forward beyond coagonism in providing enhanced efficacy and safety with less likelihood for gastrointestinal distress, a common adverse effect of GLP-1 analogs, as the individual contribution of GLP-1 agonism can be diminished. We believe the

high-potency, inherent mixed agonism within the triagonist advantageously lessens the respective target receptor occupancy rates, which more closely resembles a physiological response.

We confirmed constituent activity and demonstrated its contribution to the overall metabolic efficacy of the triagonist through indirect and direct means. Indirectly, we showed this through the comparison of *in vivo* metabolic profile of the triagonist to a matched set of the three possible coagonist combinations. Directly, we confirmed constituent activity through *in vitro* assays in target cell populations and *in vivo* studies using acute antagonist challenges and chronic studies in individual receptor–knockout mice. These results demonstrated that the triagonist possesses selected and independent pharmacological virtues indicative of each hormone, such that these otherwise independent virtues synergize to achieve superior metabolic efficacy. The thermogenic properties of glucagon supplements the body weight lowering of dual incretin action, and the additional glycemic efficacy of GIP supports GLP-1 to further buffer against the inherent hyperglycemic risk of integrated glucagon action. Through a series of imbalanced triagonists with a step-wise selective blunting of glucagon activity, we also demonstrated that glucagon activity that is aligned with GLP-1 and GIP activity is necessary for the maximal weight loss induced by the triagonist, but dampening the glucagon activity can promote better glycemic outcomes, albeit with less weight loss. However, in no instance did we witness elevation of glucose when using the balanced triagonist alone or in combination with the dual incretin coagonist with supplemental glucagon agonism, even at levels where the glucagon was much in excess. This stands in contrast to our prior observations in which the specific ratio of glucagon activity relative to GLP-1 monoagonism was of central importance to body weight lowering and the propensity to elevate glucose[28].

Through studies using individual receptor–knockout mice, we were able to clearly demonstrate the presence of each constituent activity within the triagonist, and we were also able to ascertain some of the contribution of each constituent to the overall metabolic benefits induced by the triagonist. In both *Glp1r*$^{-/-}$ and *Gcgr*$^{-/-}$ mice, we observed that loss of GLP-1 and glucagon functionality results in reduced weight-lowering efficacy. Additionally, in *Glp1r*$^{-/-}$ and *Gipr*$^{-/-}$ mice, we observed that a loss of individual incretin functionality results in differing degrees of buffering against a glucagon-mediated negative impact on blood glucose. At minimum, the studies in the individual receptor–knockout mice clearly demonstrated the presence of each constituent activity within the triagonist, but gaining insight into the contribution of each to the overall metabolic benefits elicited by the triagonist is less clear. This is mostly owing to the altered physiology that is the result of compensatory mechanisms arising from germline knockout. As just one example, *Glp1r*$^{-/-}$ (ref. 29), *Gipr*$^{-/-}$ (ref. 26) and *Gcgr*$^{-/-}$ (ref. 27) mice are all protected from HFD-induced adiposity and have differential glucose and insulin sensitivities. Together, the body weight phenotypes of all three knockout models would suggest that all three receptors should be targets of inhibition to gain beneficial effects on body composition, which is certainly not the case and should give warning to investigators that pharmacological outcomes of a particular target are often difficult to predict from targeted mutation models. Furthermore, the altered enteroendocrine responses in these three knockout lines contribute to the observed phenotypes, which here confound interpretations of data to determine the overall contributions of each component of the triagonist. Ultimately, in terms of demonstrating *in vivo* constituent activity and understanding how activity contributes to the overall effect of polyagonists, we believe there is no equivalent to a set of chemically matched analogs in which a single component activity has been deleted and subsequently tested in wild-type animals. Together with the arduous use of selective antagonists in wild-type conditions, albeit with its own limitations, these sets of reagents can circumvent the liabilities associated with the use of germline knockout models.

The magnitude of weight loss in a clinical setting and the speed with which it is achieved needs to be thoroughly established in subsequent development work. Intensive toxicological analyses are warranted, including a thorough assessment of effects on the cardiovascular system, as recent reports suggest direct chronotropic action of GLP-1R[30] and GcgR[31] agonism . In addition to cardiovascular outcomes, a thorough assessment of long-term outcomes on diabetic ketoacidosis is warranted because of the observed high degree of weight loss and reduction of circulating insulin induced in these preclinical studies. The therapeutic index of these peptides for chronic human use cannot be accurately determined from these preclinical studies; however, in long-term efficacy studies and follow-up analysis after treatment cessation, we witnessed sustained efficacy with no apparent adverse pharmacology. If it proves in subsequent testing that less aggressive glucagon agonism is preferable for long-term dosing, it is possible that the series of imbalanced triagonists with a selective titration of glucagon activity might ultimately prove to be more suitable therapeutics. Notably, the glucagon activity can be selectively fine-tuned with minimal structural or chemical change (a single amino acid change at position 3), providing the opportunity for a more personalized medicinal approach to obesity therapy that reflects the heterogeneous nature of the human condition. In entering the translational stage, the ability to choose among several options that differ in their inherent molecular pharmacology increases the likelihood of ultimate success, as well as the opportunity to explore nonconventional uses, such as for Prader-Willi syndrome, neurodegenerative diseases or nondiabetes liver diseases associated with excessive fat deposition.

Our results call into question previous reports of purported unimolecular triagonists where the body weight lowering was paltry relative to what we have observed and unsupportive of concerted triple agonism at GLP-1R, GIPR and GcgR[24,25,32]. In the most recent report[25], the total reported weight loss after three weeks of twice-daily administration was no more than 3% relative to vehicle control at a total dose of 50 nmol kg$^{-1}$ d$^{-1}$. Our synthesis of these purported triagonists and subsequent *in vitro* analysis revealed these peptides to be dramatically reduced in potency relative to the native hormones (nearly 100-fold) and to our triagonist (nearly 1,000-fold), and also failed to achieve aligned activity balance across the three receptors. These *in vitro* results suggest a basis for their limited body weight lowering relative to our more extensive results presented herein. Here, we confirmed that these compounds provide negligible metabolic benefits in DIO mice and thus do not biochemically qualify to be characterized as triagonists. Consequently, we believe that the peptides presented here represent the first discovery of balanced triagonists and that YAG-glucagon[24] and [$_{D}$A$^{2}$]GLP-1/GcG[25] do not offer relevant triple agonism.

We report the discovery of a peptide with balanced superpotency at three different metabolically relevant receptor targets: GcgR, GLP-1R and GIPR. To our knowledge, this unimolecular triagonist represents the only pharmacotherapy to date that can achieve such preclinical efficacy at such low doses to rectify obesity and its metabolic complications in rodents. It is becoming increasingly evident that adjusted enteroendocrine responses contribute to the massive and rapid metabolic improvements achieved by bariatric surgeries[33], which suggests that the simultaneous and encompassing modulation of these molecular pathways may offer a pharmacological opportunity to replicate the

altered physiology seen with bariatric surgery. Accordingly, we believe the bundled multiagonism within this single molecule embodies such a physiological-mimicking polypharmacy. The metabolic improvements elicited by the triagonist rival those induced by bariatric surgery, at least when compared to the published reports in rodent models, albeit without the consequential surgical risks and invasiveness of bariatric surgeries. Ultimately, the triagonist represents a sizable step forward beyond previous attempts of coagonism and reflects the growing notion that single-molecule polytherapies are emerging as the gold standard for obesity and diabetes medicines[13]. It is conceivable that this newly discovered triagonist could be used to deepen and broaden the efficacy in targeting of nuclear hormones[11] or find application in combination with other protein-based therapeutics[34] as we search for that pharmacology that more closely replicates physiology in the pursuit of medicinal alternatives to bariatric surgery.

## METHODS

Methods and any associated references are available in the online version of the paper.

*Note: Any Supplementary Information and Source Data files are available in the online version of the paper.*


### ACKNOWLEDGMENTS

We thank J. Levy for technical and chemical support of peptide synthesis. We thank J. Ford for cell culture maintenance. We thank J. Patterson, J. Day, B. Ward and C. Ouyang for discussions on chemical structure-activity relationships and seminal work in mixed agonist peptides. We thank J. Holland, J. Hembree, C. Raver, S. Amburgy, J. Pressler, J. Sorrell, D. Küchler and L. Sehrer for assistance during *in vivo* pharmacological studies. At F. Hoffmann–La Roche Ltd., we thank A. Roeckel, A. Vandjour and E. Hainaut for assistance during *in vivo* pharmacological studies; M. Brecheisen, C. Richardson, G. Branellec and V. Ott for necropsy and immunohistological procedures; C. Apfel, C. Wohlgesinger and V. Griesser for bioanalytics; and M. Kapps, C. Flament, P. Schrag, C. Rapp, M.S. Gruyer, V. Dall'Asen, F. Schuler and M. Otteneder for assistance in pharmacokinetic studies. We thank M. Charron (Albert Einstein College of Medicine) for providing *Gcgr*$^{-/-}$ mice and Y. Seino (Kansai Electric Power Hospital) for providing *Gipr*$^{-/-}$ mice. Partial research funding was provided by Marcadia Biotech, which has been acquired by F. Hoffmann–La Roche Ltd., and by grants from the Deutsche Forschungsgesellschaft (DFG; TS226/1-1), Deutsches Zentrum für Diabetesforschung (DZD), EurOCHIP (FP-7-HEALTH-2009-241592), Helmholtz Alliance ICEMED–Imaging and Curing Environmental Metabolic Diseases (through the Initiative and Networking Fund of the Helmholtz Association) and the Canadian Institutes of Health Research (93749).


### AUTHOR CONTRIBUTIONS

B.F. designed and performed *in vitro, in vivo* and *ex vivo* rodent experiments, synthesized and characterized compounds, analyzed and interpreted data, and co-wrote the manuscript. B.Y. designed, synthesized and characterized compounds, performed *in vitro* experiments, and analyzed and interpreted data. N.O. designed and led *in vivo* pharmacology and metabolism rodent studies and interpreted data. D.P.-T., P.T.P., K.M.H., J.E.C., D.S., R.J.S., C.C., D.J.D., E.S., A.K. and T.D.M. designed, supervised and performed *in vivo* experiments and interpreted data. L.Z. designed *in vivo* experiments and interpreted data. K.F. performed *in vivo* experiments. J.C. and D.L.S. designed, synthesized and characterized compounds. K.B. designed and synthesized compounds. S.U., W.R., C.H., E.S., K.C.-K. and A.K. designed and performed *in vivo* and *ex vivo* analyses in ZDF rats and interpreted data. J.F. performed liver histology and interpreted data. S.U. performed pancreas histology and interpreted data. C.H., A.K. and V.G. designed and performed *in vitro* experiments and interpreted data. S.B. led pharmacokinetic studies and interpreted data. R.D.D. and M.H.T. conceptualized, designed and interpreted all studies and wrote the manuscript together with B.F.

### COMPETING FINANCIAL INTERESTS

The authors declare competing financial interests: details are available in the online version of the paper.




1. Speakman, J.R. & O'Rahilly, S. Fat: an evolving issue. *Dis. Model. Mech.* **5**, 569–573 (2012).
2. Di Dalmazi, G., Vicennati, V., Pasquali, R. & Pagotto, U. The unrelenting fall of the pharmacological treatment of obesity. *Endocrine* **44**, 598–609 (2013).
3. Rodgers, R.J., Tschop, M.H. & Wilding, J.P. Anti-obesity drugs: past, present and future. *Dis. Model. Mech.* **5**, 621–626 (2012).
4. Gadde, K.M. *et al.* Effects of low-dose, controlled-release, phentermine plus topiramate combination on weight and associated comorbidities in overweight and obese adults (CONQUER): a randomised, placebo-controlled, phase 3 trial. *Lancet* **377**, 1341–1352 (2011).
5. Allison, D.B. *et al.* Controlled-release phentermine/topiramate in severely obese adults: a randomized controlled trial (EQUIP). *Obesity (Silver Spring)* **20**, 330–342 (2012).
6. Garvey, W.T. *et al.* Two-year sustained weight loss and metabolic benefits with controlled-release phentermine/topiramate in obese and overweight adults (SEQUEL): a randomized, placebo-controlled, phase 3 extension study. *Am. J. Clin. Nutr.* **95**, 297–308 (2012).
7. Fosgerau, K. *et al.* The novel GLP-1-gastrin dual agonist, ZP3022, increases beta-cell mass and prevents diabetes in db/db mice. *Diabetes Obes. Metab.* **15**, 62–71 (2013).
8. Day, J.W. *et al.* A new glucagon and GLP-1 coagonist eliminates obesity in rodents. *Nat. Chem. Biol.* **5**, 749–757 (2009).
9. Finan, B. *et al.* Unimolecular dual incretins maximize metabolic benefits in rodents, monkeys, and humans. *Sci. Transl. Med.* **5**, 209ra151 (2013).
10. Pocai, A. *et al.* Glucagon-like peptide 1/glucagon receptor dual agonism reverses obesity in mice. *Diabetes* **58**, 2258–2266 (2009).
11. Finan, B. *et al.* Targeted estrogen delivery reverses the metabolic syndrome. *Nat. Med.* **18**, 1847–1856 (2012).
12. Clemmensen, C. *et al.* GLP-1/glucagon co-agonism restores leptin responsiveness in obese mice chronically maintained on an obesogenic diet. *Diabetes* **63**, 1422–1427 (2014).
13. Sadry, S.A. & Drucker, D.J. Emerging combinatorial hormone therapies for the treatment of obesity and T2DM. *Nat. Rev. Endocrinol.* **9**, 425–433 (2013).
14. Barrera, J.G., Sandoval, D.A., D'Alessio, D.A. & Seeley, R.J. GLP-1 and energy balance: an integrated model of short-term and long-term control. *Nat. Rev. Endocrinol.* **7**, 507–516 (2011).
15. Campbell, J.E. & Drucker, D.J. Pharmacology, physiology, and mechanisms of incretin hormone action. *Cell Metab.* **17**, 819–837 (2013).
16. Habegger, K.M. *et al.* The metabolic actions of glucagon revisited. *Nat. Rev. Endocrinol.* **6**, 689–697 (2010).
17. Habegger, K.M. *et al.* Fibroblast growth factor 21 mediates specific glucagon actions. *Diabetes* **62**, 1453–1463 (2013).
18. Chabenne, J.R., DiMarchi, M.A., Gelfanov, V.M. & DiMarchi, R.D. Optimization of the native glucagon sequence for medicinal purposes. *J. Diabetes Sci. Technol.* **4**, 1322–1331 (2010).
19. Ward, B. *et al.* Peptide lipidation stabilizes structure to enhance biological function. *Mol. Metab.* **2**, 468–479 (2013).
20. Yip, R.G., Boylan, M.O., Kieffer, T.J. & Wolfe, M.M. Functional GIP receptors are present on adipocytes. *Endocrinology* **139**, 4004–4007 (1998).
21. Panjwani, N. *et al.* GLP-1 receptor activation indirectly reduces hepatic lipid accumulation but does not attenuate development of atherosclerosis in diabetic male ApoE$^{-/-}$mice. *Endocrinology* **154**, 127–139 (2013).
22. Patterson, J.T. *et al.* A novel human-based receptor antagonist of sustained action reveals body weight control by endogenous GLP-1. *ACS Chem. Biol.* **6**, 135–145 (2011).
23. European Medicines Agency. Assessment Report for Victoza; doc. ref. EMEA/379172/2009 (2009).
24. Bhat, V.K., Kerr, B.D., Vasu, S., Flatt, P.R. & Gault, V.A.A. DPP-IV-resistant triple-acting agonist of GIP, GLP-1 and glucagon receptors with potent glucose-lowering and insulinotropic actions in high-fat-fed mice. *Diabetologia* **56**, 1417–1424 (2013).
25. Gault, V.A., Bhat, V.K., Irwin, N. & Flatt, P.R. A novel GLP-1/glucagon hybrid peptide with triple-acting agonist activity at GIP, GLP-1 and glucagon receptors and therapeutic potential in high-fat-fed mice. *J. Biol. Chem.* **288**, 35581–35591 (2013).
26. Miyawaki, K. *et al.* Inhibition of gastric inhibitory polypeptide signaling prevents obesity. *Nat. Med.* **8**, 738–742 (2002).
27. Gelling, R.W. *et al.* Lower blood glucose, hyperglucagonemia, and pancreatic alpha cell hyperplasia in glucagon receptor knockout mice. *Proc. Natl. Acad. Sci. USA* **100**, 1438–1443 (2003).
28. Day, J.W. *et al.* Optimization of co-agonism at GLP-1 and glucagon receptors to safely maximize weight reduction in DIO-rodents. *Biopolymers* **98**, 443–450 (2012).
29. Scrocchi, L.A. & Drucker, D.J. Effects of aging and a high fat diet on body weight and glucose tolerance in glucagon-like peptide-1 receptor$^{-/-}$ mice. *Endocrinology* **139**, 3127–3132 (1998).
30. Kim, M. *et al.* GLP-1 receptor activation and Epac2 link atrial natriuretic peptide secretion to control of blood pressure. *Nat. Med.* **19**, 567–575 (2013).
31. Mukharji, A., Drucker, D.J., Charron, M.J. & Swoap, S.J. Oxyntomodulin increases intrinsic heart rate through the glucagon receptor. *Physiol. Rep.* **1**, e00112 (2013).
32. Bhat, V.K., Kerr, B.D., Flatt, P.R. & Gault, V.A. A novel GIP-oxyntomodulin hybrid peptide acting through GIP, glucagon and GLP-1 receptors exhibits weight reducing and anti-diabetic properties. *Biochem. Pharmacol.* **85**, 1655–1662 (2013).
33. Ionut, V., Burch, M., Youdim, A. & Bergman, R.N. Gastrointestinal hormones and bariatric surgery-induced weight loss. *Obesity (Silver Spring)* **21**, 1093–1103 (2013).
34. Muller, T.D. *et al.* Restoration of leptin responsiveness in diet-induced obese mice using an optimized leptin analog in combination with exendin-4 or FGF21. *J. Pept. Sci.* **18**, 383–393 (2012).

## ONLINE METHODS

**Peptide synthesis.** Peptides were synthesized by solid-phase peptide synthesis methods using *in situ* neutralization for both Boc-based and Fmoc-based chemistries. For Boc-based neutralization peptide synthesis, 0.2 mmol 4-methylbenzhydrylamine (MBHA) resin (Midwest Biotech) was used on a highly modified Applied Biosystems 430A peptide synthesizer by standard Boc methods using DEPBT/DIEA for coupling and TFA for deprotection of amino-terminal amines. Peptidyl resins were treated with hydrofluoric (HF) acid/*p*-cresol (10:0.5 vol/vol) at 0 °C for 1 h with agitation. HF was removed *in vacuo* and precipitated the cleaved and deprotected peptide in diethyl ether. For Fmoc-based neutralization peptide synthesis, 0.1 mmol Rink MBHA resin (Novabiochem) was used on an Applied Biosystems 433A peptide synthesizer by standard Fmoc methods using DIC/$Cl^-$HOBt for coupling and 20% piperidine/dimethylformamide (DMF) for deprotection of N-terminal amines. Completed peptidyl resins were treated with TFA/TIS/anisole (9:0.5:0.5 vol/vol/v) for 2 h with agitation. After removal of the ether, the crude peptide was dissolved in aqueous buffer containing at least 20% acetonitrile (ACN) and 1% acetic acid (AcOH) before lyophilization. Peptide molecular weights were confirmed by electrospray ionization (ESI) or matrix-assisted laser desorption/ionization time-of-flight (MALDI-TOF) mass spectrometry (summarized in **Supplementary Table 1**) and character confirmed by analytical reversed-phase HPLC in 0.1% TFA with an ACN gradient on a Zorbax C8 or C18 column (0.46 × 5 cm).

**Peptide purification.** Following cleavage from the resin, crude extracts were purified by semi-preparative reversed-phase HPLC in 0.1% TFA with an ACN gradient on a Vydac C8 column (2.2 × 25 cm). Preparative fractions were analyzed for purity by analytical reversed-phase HPLC using the conditions listed above. Peptide molecular weights were confirmed by ESI or MALDI-TOF mass spectrometry. Purified peptides were lyophilized, aliquotted, and stored at 4 °C.

**Cell lines.** All cell lines used were confirmed to be mycoplasma free and tested on a monthly basis. Parent HEK-293 cells used for *in vitro* receptor activity were obtained from the ATCC. MIN6, 3T3-L1, and rat hepatocytes were obtained from internal stock at F. Hoffmann-La Roche. None of the cell lines were authenticated in house by short tandem repeat (STR) DNA profiling.

**Human GLP-1, GIP, and glucagon receptor activation.** Each peptide was individually tested for its ability to activate the GLP-1, GIP, or glucagon receptor through a cell-based luciferase reporter gene assay that indirectly measures cAMP induction. Human embryonic kidney (HEK293) cells were co-transfected with each individual receptor cDNA (zeocin-selection) and a luciferase reporter gene construct fused to a cAMP response element (CRE) (hygromycin B-selection). Cells were seeded at a density of 22,000 cells per well and serum deprived for 16 h in DMEM (HyClone) supplemented with 0.25% (vol/vol) bovine growth serum (BGS) (HyClone). Serial dilutions of the peptides were added to 96-well cell-culture treated plates (BD Biosciences) containing the serum-deprived, co-transfected HEK293 cells, and incubated for 5 h at 37 °C and 5% $CO_2$ in a humidified environment. To stop the incubation, an equivalent volume of Steady Lite HTS luminescence substrate reagent (PerkinElmer) was added to the cells to induce lysis and expose the lysates to luciferin. The cells were agitated for 5 min and stored for 10 min in the dark. Luminescence was measured on a MicroBeta-1450 liquid scintillation counter (PerkinElmer). Luminescence data were graphed against concentration of peptide and $EC_{50}$ values were calculated using Origin software (OriginLab).

**Mouse, rat, and cynomolgus monkey receptor activation.** CHO-K1 cells were transiently transfected with expression plasmids constructed from pcDNA3.1 plasmids (Life Technologies) containing the native sequence for each individual receptor originating from mouse, rat, and cynomolgus monkey, which were based on reference database sequences, as well as an artificial Kozak sequence (GCCGCCATCATG) to further aid expression. CHO-K1 cells were cultured in Ham's F-12 media (GIBCO) supplemented with 10% FBS, 2 mM glutathione, 500 µg/ml Geneticin, 100 µg/ml penicillin and 100 µg/ml streptomycin. cAMP production was assessed following the method below.

**cAMP assay.** Mouse insulinoma MIN6 cells were cultured in RPMI 1640 medium supplemented with 10% FBS (PAA Laboratories), 10 mM HEPES, 1 mM sodium pyruvate, 50 µM 2-β-mercaptoethanol, 100 µg/ml penicillin and 100 µg/ml streptomycin and were grown at 37 °C and 5% $CO_2$ in a humidified incubator. Rat hepatocytes were thawed from cryopreserved stock immediately before the experiment. Mouse 3T3-L1 cells were grown in DMEM/10% FBS and 1% penicillin/streptomycin in a humidified incubator with 5% $CO_2$ at 37 °C. Confluent 3T3-L1 cells were initiated to differentiate with DMEM containing 20% FBS, 0.5 mM IBMX, 0.4 µg/ml dexamethasone and 5 µg/ml insulin. After 5 days, media was replaced with DMEM containing 20% FBS, 4 µg/ml insulin and 10 µM rosiglitazone. After 3 days, media was replaced with DMEM containing 10% FBS. Cells were used 10 days after initiation of differentiation.

For cAMP production assessment, the medium was removed and the cells were washed with PBS. For MIN6 cells, cell monolayers were incubated for 5 min at 37 °C with 5 mL Cell Dissociation solution (Gibco) to dislodge the cells. For suspended MIN6 cells and fresh rat hepatocytes, cells were transferred to a 96-well plate at a seeding density of 5000 cells/well. For 3T3-L1 cells, cells were seeded directly into 96-well plates and differentiated. The cell suspension (MIN6 and hepatocytes) or the cell monolayer (3T3-L1) was then incubated for 30 min at room temperature with the peptides. The reaction was stopped by addition of lysis buffer and cAMP generated was determined using the cAMP Dynamic 2 Kit (Cisbio) following the manufacturer's instructions. The time-resolved fluorescence signal was determined using an EnVision (PerkinElmer), and cAMP production was calculated based on standard curve run in parallel for every experiment. Data were analyzed using GraphPad Prism.

**CEREP assay for non-selective receptor binding.** The cross-reactive binding of triagonist was profiled in a high-throughput custom-made competitive binding screen at 73 targets, including GLP-1R and GcgR as positive controls (Cerep). The exact specifications of each individual assay are detailed in **Supplementary Table 3**, which includes receptor source, labeled and unlabeled ligands, and incubation conditions. The specific ligand binding to the respective receptors is defined as the difference between the total binding and the non-specific binding determined in the presence of an excess of a respective native, unlabeled ligand. Results are expressed as percentage specific binding, calculated by [(triagonist specific binding / control specific binding) × 100], and also as percentage inhibition of control, calculated by [100 – (triagonist specific binding / control specific binding) × 100]. In general, results showing a percentage inhibition of control that is greater than 25% is considered a positive result of specific receptor binding, and values less than 25% are considered a negative result of specific receptor binding.

**General experimental approaches for *in vivo* pharmacology experiments.** For *in vivo* pharmacological studies, a group size of eight was preferentially used, which was determined from previous experiments where we determined this to be optimal for *in vivo* evaluation. Smaller group sizes were used in the studies utilizing genetically modified animals because there were not sufficient numbers available to reach a group size of eight. For studies using lean and obese mice, mice were randomized into the treatment groups based upon body weight and body fat/lean mass and levels of blood glucose. Rodents were single- or group-housed on a 12-h/12-h light-dark cycle at 22 °C with free access to food and water. Group size estimations were based upon a power calculation to minimally yield an 80% chance to detect a significant difference in body weight of $P < 0.05$ between the treatment groups. For studies using diabetic rodents, rodents were randomized based on body weight, body fat/lean mass, and levels of blood glucose. The investigators were not blinded during group allocation or during *in vivo* profiling of compounds. No samples or animals were excluded from the longitudinal *in vivo* pharmacological profiling, challenge tests, or port mortem analysis. The age and strain of the mice are indicated below and in the figure legends.

**DIO mice.** With all DIO mice, male C57BL/6 mice (Jackson Laboratories) were fed a diabetogenic diet (Research Diets), which is a high-sucrose diet with 58% kcal from fat, 25.5% kcal from carbohydrates, and 16.4% kcal from protein, beginning at 8 weeks or 2 months of age. DIO mice were single- or group-housed on a 12-h/12-h light-dark cycle at 22 °C with free access to food and water.

Mice were maintained under these conditions for a minimum of 16 weeks before initiation of pharmacological studies and were between the ages of 6 months and 18 months old. All injections and tests were performed during the light cycle. Mice were randomized and evenly distributed to test groups according to body weight and body composition. No animals were excluded due to illness or outlier results; therefore, no exclusion determination was required. If *ex vivo* molecular biology/histology/biochemistry analyses were performed, the entire group of mice for each treatment was analyzed.

***Glp1r*$^{-/-}$ mice.** Male *Glp1r*$^{-/-}$ mice and wild-type littermates (C57BL/6 background) were bred in house and fed the aforementioned diabetogenic diet for 12 weeks before initiation of injections. All tests were performed on mice aged 8 months and injections were administered during the light cycle. Mice were single- or group-housed on a 12-h/12-h light-dark cycle at 22 °C with free access to food and water.

***Gcgr*$^{-/-}$ mice.** Male *Gcgr*$^{-/-}$ mice and wild-type littermates (C57BL/6 background) were bred in house and, starting at 12 weeks of age, were fed the aforementioned diabetogenic diet for 6 weeks before initiation of injections. All tests were performed on mice aged 5 months and injections were administered during the light cycle. Mice were single- or group-housed on a 12-h/12-h light-dark cycle at 22 °C with free access to food and water.

***Gipr*$^{-/-}$ mice.** Male *Gipr*$^{-/-}$ mice and wild-type littermates (C57BL/6 background) were bred in house and, starting at 12 weeks of age, were fed the aforementioned diabetogenic diet for 6 weeks before initiation of injections. All tests were performed on mice aged 5 months and injections were administered during the light cycle. Mice were single- or group-housed on a 12-h/12-h light-dark cycle at 22 °C with free access to food and water.

**db/db mice.** Six-week-old male *db/db* mice (Jackson Laboratories; C57BL/6 background) were housed 4 per cage and provided access to standard chow diet and water *ad libitum*. Mice were 9 weeks old when used for the indicated studies. Mice were randomized by *ad libitum*–fed blood glucose and body weight, and were double-housed for the study. All injections and tests were performed during the light cycle.

**STZ mice.** Thirteen-month-old male C57BL/6 mice (Jackson Laboratories) were housed 4 per cage and provided access to standard chow diet and water *ad libitum.* Streptozotocin was administered at a dose of 150 mg per kg body weight via a single intraperitoneal injection. After 3 d, mice with a blood glucose level exceeding 200 mg/dl were considered sufficiently diabetic and were treated with long-acting insulin (made in house) via daily subcutaneous injections for 4 weeks to maintain euglycemia. Mice were used for the glucagon challenge test after a 72-h washout period of the insulin and were randomized based on *ad libitum*–fed blood glucose and body weight. For the challenge test, mice were subjected to 6 h of fasting at the onset of the light cycle and injected intraperitoneally with GcgR antagonist 15 min before administration of the triagonist. Tail blood glucose concentrations were measured using a handheld glucometer (TheraSense FreeStyle) before antagonist administration (−15 min), before triagonist administration (0 min), and at 15, 30, 60, and 120 min after injection of the triagonist. All injections and tests were performed during the light cycle.

**DIO rats.** Twelve-week-old male Long Evens rats were fed a diabetogenic diet (Research Diets), which is a high-sucrose diet with 58% kcal from fat, for 40 weeks before initiating the long-term study. The DIO rats were single-housed on a 12:12-h light-dark cycle at 22 °C with free access to food and water. Rats were randomized and distributed to test groups according to body weight and body composition. All injections and tests were performed during the light cycle.

**ZDF rats.** Nine-week-old male ZDF rats (Charles River Laboratories, USA) were fed a special diet (Purina PMI 5008) and housed 1 per cage at room temperature (~21 °C) and relative humidity 55–65%. A 12-h light-dark cycle was maintained in the rooms with all tests being performed during the light phase. Access to food and water was *ad libitum*. After 2 weeks of acclimatizing, measurement of fasting blood glucose concentrations for randomization was performed by tail puncture in conscious animals. ZDF rats were distributed into groups ($n = 8$/group) according to body weight and fasting glucose concentrations. Immediately after treatment cessation, $n = 4$ rats per group were blindly selected for *ex vivo* analysis. The remaining $n = 4$ rats were monitored for 21 additional days after treatment termination and were subsequently killed for *ex vivo* analysis.

**Ethical approval.** All rodent studies were approved by and performed according to the guidelines of the Institutional Animal Care and Use Committee of the Helmholtz Center Munich, University of Cincinnati, and under an animal research protocol (ARP) authorization to F. Hoffmann-La Roche by the Swiss Cantonal Veterinary Office Basel-Stadt and in accordance with guidelines of the Association for the Assessment and Accreditation of Laboratory and Animal Care (AAALAC unit no. 001057) and appropriate federal, state and local guidelines.

**Rodent pharmacological and metabolism studies.** Compounds were administered by repeated subcutaneous injections in the middle of the light phase at the indicated doses with the indicated durations. Co-administration of compounds was administered by single formulated injections. Body weights and food intake were measured every day or every other day after the first injection. All studies in wild-type mice were performed with a group size of $n = 8$ per group using mice on a C57BL6 background. Fasted blood glucose was measured upon study initiation and termination following 6 h of fasting. For assessment of glucose and insulin tolerance during chronic treatment, the challenge tests were performed at least 24 h after the last administration of compounds. The investigators were not blinded to group allocation during the *in vivo* experiments or to the assessment of experimental end points.

**Body composition measurements.** Whole-body composition (fat and lean mass) was measured using nuclear magnetic resonance technology (EchoMRI).

**Energy balance physiology measurements.** Energy intake, energy expenditure, and home-cage activity were assessed using a combined indirect calorimetry system (TSE Systems). $O_2$ consumption and $CO_2$ production were measured every 10 min for a total of 120 h (including 48 h of adaptation) to determine the respiratory quotient and energy expenditure after an initial treatment regimen for 2 weeks. Food intake was determined continuously for 120 h at the same time as the indirect calorimetry assessments by integration of scales into the sealed cage environment. Home-cage locomotor activity was determined using a multidimensional infrared light beam system with beams scanning the bottom and top levels of the cage, and activity being expressed as beam breaks.

**Blood parameters.** Blood was collected after a 6-h fast from tail veins or after euthanasia using EDTA-coated microvette tubes (Sarstedt), immediately chilled on ice, centrifuged at 5,000*g* and 4 °C, and plasma stored at −80 °C. Plasma insulin was quantified by a radioimmunoassay from Linco (Sensitive Rat Insulin RIA; Linco Research) or by an ELISA assay (Alpco). Plasma FGF21, adiponectin, GIP, GLP-1, and glucagon were quantified by an ELISA assay (Millipore). Plasma cholesterol, triglycerides, ALT, and AST were measured using enzymatic assay kits (Thermo Fisher). Plasma free fatty acids and ketones were measured using enzymatic assay kits (Wako). All assays were performed according to the manufacturers' instructions.

**Acute glucose tolerance test with GLP-1R antagonist.** For the determination of the effects of the triagonist on intraperitoneal glucose tolerance with concomitant antagonism of the GLP-1R, 6-h fasted male C57BL/6 DIO mice ($n = 8$ per group; age 9 months) were pretreated with vehicle or the GLP-1R antagonist (1 µmol per kg body weight) via an intraperitoneal injection 30 min before the intraperitoneal glucose challenge (2 g of glucose per kg body weight). Vehicle or the triagonist (1 nmol per kg body weight) was administered 15 min before the glucose challenge via intraperitoneal injections. Tail blood glucose concentrations were measured by using a handheld glucometer (TheraSense FreeStyle) before subsequent injections at −30, −15, 0, 15, 30, 60, and 120 min after the glucose administration.




doi:10.1038/nm.3761

**Acute glucose tolerance test with GIPR antagonist.** For the determination of the effects of the triagonist on intraperitoneal glucose tolerance with concomitant antagonism of the GIPR, 6-h fasted male *Glp1r*$^{-/-}$ DIO mice ($n$ = 8 per group; age 12 months) were pretreated with vehicle or the GIPR antagonist (2 µmol per kg body weight) via an intraperitoneal injection 30 min before the intraperitoneal glucose challenge (1.5 g of glucose per kg body weight). Vehicle or the triagonist (2 nmol per kg body weight) was administered 15 min before the glucose challenge via intraperitoneal injections. Tail blood glucose concentrations were measured by using a handheld glucometer (TheraSense FreeStyle) before subsequent injections at −30, −15, 0, 15, 30, 60, and 120 min after the glucose administration.

**Acute glucose tolerance test with GcgR antagonist.** For the determination of the effects of the triagonist on glycemia with concomitant antagonism of the GcgR, 6-h fasted male STZ C57BL/6 lean mice ($n$ = 8 per group; age 13 months) were pretreated with vehicle or the GcgR antagonist (1 µmol per kg body weight) via an intraperitoneal injection 15 min before the intraperitoneal injection with vehicle or the triagonist (1 nmol per kg body weight). Tail blood glucose concentrations were measured by using a handheld glucometer (TheraSense FreeStyle) before subsequent injections at −15, 0, 15, 30, 60, and 120 min after the glucose administration.

**Glucose tolerance test.** For the determination of glucose tolerance, mice were subjected to 6 h of fasting at the onset of the light cycle and injected intraperitoneally with 1.5 g glucose per kg body weight for DIO mice or 2 g glucose per kg body weight for lean mice (20% w/v d-glucose (Sigma) in 0.9% w/v saline). For acute glucose tolerance tests using antagonists, the antagonists, at a 1000-fold excess dose of the triagonist, were administered 15 min before agonist administration and 30 min before the glucose challenge. For *db/db* mice, mice were subjected to 6 h of fasting at the onset of the light cycle and injected intraperitoneally with 1 g glucose per kg body weight. Tail blood glucose concentrations were measured using a handheld glucometer (TheraSense FreeStyle) before (0 min) and at 15, 30, 60, and 120 min after injection. For the acute effects of the triagonist with or without respective antagonists, blood glucose concentrations were measured before administration of the antagonist (−30 min) and the triagonist (−15 min) in addition to the measurement times listed above. For ZDF rats, oral glucose tolerance was assessed in 8 rats per group after an overnight fasting period (16 h) and blood glucose was measured before oral glucose challenge (2 g kg$^{-1}$), and subsequently at 15, 30, 60 and 120 min post-glucose challenge. Blood glucose was monitored using the AccuCheck glucometer system.

**Insulin tolerance test.** For the determination of insulin tolerance, mice were subjected to 6 h of fasting at the onset of the light cycle and injected intraperitoneally with 0.75 units of insulin per kg body weight. Tail blood glucose concentrations were measured by using a handheld glucometer (TheraSense FreeStyle) before (0 min) and at 15, 30, 60, and 120 min after injection.

**Histopathology and immunohistochemistry.** The methodology has been described[35,36]. In brief, tissue samples were fixed in 10% neutral-buffered formalin for 24h, dehydrated and subsequently embedded into paraffin. Standard hematoxylin and eosin staining was performed to assess liver histology. The following immunofluorescence stainings on tissue sections of 4µm were carried out to assess islet morphology: anti-insulin (1:50; Dako; A0564), anti-glucagon (1:50; Dako; A0565) and 4′, 6-diamidino-2-phenylindole (DAPI; 1:1,000; Roche; 10236276001), followed by respective secondary fluorescent antibodies (Alexa Fluor). Digital imaging fluorescence microscopy of the pancreas was performed using a scanning platform (MetaSystems) with a Zeiss Imager Z.2 microscope (Carl Zeiss MicroImaging, Inc.). Quantitative image analysis of islet morphology was performed using Definiens Architect XD (Definiens AG). Investigators were not blinded during analysis.

**Triagonist pharmacokinetic studies.** All pharmacokinetic studies were conducted with the approval of the local veterinary authority in strict adherence to the Swiss federal regulations on animal protection and to the rules of the Association for Assessment and Accreditation of Laboratory Animal Care International (AAALAC). Studies with rodents and nonhuman primates were conducted according to Roche animal permissions for performing PK studies at Roche Basel. Adult male C57BL/6J mice weighing approximately 30 g each (Harlan Laboratories), adult male DIO mice weighing approximately 60 g each (Charles River), and adult male Wistar rats weighing approximately 250 g each (Harlan Laboratories) were housed in a controlled environment (temperature, humidity, and 12-h light/dark cycle) with free access to food and water. Six adult male cynomolgus monkeys weighing approximately 10 kg each (Roche monkey PK colony) were routinely used for pharmacokinetic studies. Nonrandomized rodents were administered with the compound as subcutaneous injection in the neck (45 µg kg$^{-1}$) and nonrandomized monkeys in the flank (15 µg kg$^{-1}$). Blood from mice and rats was collected under anesthesia (5% isoflurane inhalation in pure oxygen), while no anesthesia was needed for the monkeys. Blood samples from mice ($n$ = 2 samples per time point), rats ($n$ = 3 samples per time point), and monkeys ($n$ = 3 samples per time point) were collected up to 24 h postdose by heart puncture, sublingually, or from the brachial vein, respectively, and placed on ice into EDTA-coated polypropylene tubes. Plasma was prepared from blood within 30 min by centrifugation at 3000*g* for 5 min at 4 °C and frozen immediately. All samples were stored at −20 °C. Compound concentrations in plasma were determined by LC-MS/MS and respective pharmacokinetic parameters were determined by Non-Compartmental Analysis (NCA) with the industry standard software Phoenix WinNonlin (Build 6.2.0.495, Pharsight). Researchers were not blinded during the investigation.

**GLP-1/GIP coagonist pharmacokinetic studies.** All procedures in this protocol are in compliance with the US Department of Agriculture's (USDA) Animal Welfare Act (9 CFR Parts 1, 2, and 3); the Guide for the Care and Use of Laboratory Animals, Institute of Laboratory Animal Resources, National Academy Press, Washington, D.C., 1996; and the National Institutes of Health, Office of Laboratory Animal Welfare. Studies with rodents and nonhuman primates were conducted according to Roche animal permissions for performing PK studies at Roche Basel. Whenever possible, procedures in this study are designed to avoid or minimize discomfort, distress, and pain to animals. Three adult cynomolgus monkeys were arbitrarily chosen from an in house colony and individually housed in a controlled environment on a 12-h light/dark cycle. Whole blood was collected via the femoral vein/artery at 15 min, 30 min, 1 h, 2 h, 4 h, 8 h, 12 h, 24 h, 48 h, 72 h, and 96 h after compound administration via a subcutaneous injection in the flank. Unaudited plasma and tissue pharmacokinetic analysis data were analyzed using WinNonlin, version 5.2.1 software (Pharsight, Inc.) and Microsoft Office Excel 2003. Use of Excel was limited to receipt of bioanalytical data and transfer into WinNonlin for pharmacokinetic analysis. Researchers were not blinded during the investigation.

**Statistical analyses.** Statistical analyses were performed on data distributed in a normal pattern using a regular one-way or two-way analysis of variance (ANOVA) with Tukey *post hoc* multiple comparison analysis to determine statistical significance between treatment groups. Differences with $P$ values less than 0.05 were considered significant. Group size estimations were based upon a power calculation to minimally yield an 80% chance to detect a significant difference in body weight of $P < 0.05$ between the treatment groups.

35. Bénardeau, A. *et al.* Effects of the dual PPAR-α/γ agonist aleglitazar on glycaemic control and organ protection in the Zucker diabetic fatty rat. *Diabetes Obes. Metab.* **15**, 164–174 (2013).
36. Uhles, S. *et al.* Taspoglutide, a novel human once-weekly GLP-1 analogue, protects pancreatic beta-cells *in vitro* and preserves islet structure and function in the Zucker diabetic fatty rat *in vivo*. *Diabetes Obes. Metab.* **13**, 326–336 (2011).

# Integrated triple gut hormone action broadens the therapeutic potential of endocrine biologics for metabolic diseases

Brian Finan[1–3*#], Bin Yang[3,4*], Nickki Ottaway[5], David L. Smiley[3], Tao Ma[3,6], Christoffer Clemmensen[1,2], Joe Chabenne[3,7], Lianshan Zhang[4], Kirk M. Habegger[8], Katrin Fischer[1,2], Jonathan E. Campbell[9], Darleen Sandoval[5], Randy J. Seeley[5], Konrad Bleicher[10], Sabine Uhles[10], William Riboulet[10], Jürgen Funk[10], Cornelia Hertel[10], Sara Belli[10], Elena Sebokova[10], Karin Conde-Knape[10], Anish Konkar[10], Daniel J. Drucker[9], Vasily Gelfanov[3], Paul T. Pfluger[1,2,5], Timo D. Müller[1,2], Diego Perez-Tilve[5], Richard D. DiMarchi[3#] & Matthias H. Tschöp[1,2,5#]

Nature Medicine: doi:10.1038/nm.3761

## Supplemental Results

### Chemical evolution from co-agonism to tri-agonism

The structural and sequence similarities amongst the three hormones (Fig. 1e), coupled with prior structure-function studies[1,2], informed the design of sequence hybridized peptides of high potency and balanced mixed agonism. The native hormones share nine conserved amino acids at positions 4, 5, 6, 8, 9, 11, 22, 25, and 26. These residues can be broadly grouped into two regions constituted by amino acids 4-11 and 22-26. The remaining central residues (amino acids 12-21) and the proximal terminal amino acids (1-3 and 27-30) exhibit more diversity that imparts the specificity of receptor interaction with each respective native hormone. Consequently, the challenge here is to maintain the individual affinity of each ligand for its receptor while eliminating the structural elements that convey selective preference for each individual receptor. Or stated differently, the objective here was the identification of a high affinity, promiscuous peptide for these three receptors.

Intermediary tri-agonist candidates were built from a glucagon-based core sequence with residues incorporated from GLP-1 that were previously shown to impart balanced and potent co-agonism at GLP-1R and GcgR[1]. This starting chimeric peptide features specific GLP-1 residues in the C-terminal portion at positions 17, 18, 20, 21, 23, and 24 (sequences of intermediate analogs displayed in Supplementary Figure 1 and mass spectrometry data is summarized in Supplementary Table 1). A series of peptide analogs was progressed in an iterative manner to introduce GIP agonism without destroying GLP-1R and GcgR potency. Each peptide was assessed for potency and maximal activity in a highly sensitive cell-based reporter gene assay that measured cAMP induction where one of the three human receptors was over-expressed in HEK293 cells (Table 1). In initial attempts to gain GIP activity, GIP-

specific N-terminal amino acids were individually and selectively introduced into peptide analogs of the parent, chimeric peptide. However, these GIP-derived substitutions, including $Tyr^1$ and $Ile^7$, which are well-characterized to be essential for native GIP activity[3], demonstrated little improvement in GIP potency (data not shown). Separately, $Glu^3$ substitution into the parent chimeric peptide, had noticeably enriched GIP character, but this resulted in a substantial reduction in potency at GcgR compared to the starting peptide (Table 1, peptide 9). Each of the three individual substitutions resulted in a concomitant loss of activity at the two other receptors, and in particular GcgR potency seemed most sensitive with the $Glu^3$ substitution being especially destructive, which is consistent with published reports[4,5]. This demonstrated that imparting sufficient GIP activity would not be trivial and suggested that extensive sequence modifications were essential to introduce the requisite triple agonism we desired. With the eventual intent of using these peptides for *in vivo* study, we considered the prospect of using site-specific lipidation to extend duration of biological action by promoting plasma albumin binding. As we have shown previously, site-specific lipidation can also serve as a chemical tool to enhance secondary structure and broaden biological activity[6]. We introduced a lysine at residue ten in the parent peptide to which a palmitic acid (C16:0), which was amidated through a single glutamic acid coupled at its gamma carboxylate (γE spacer). The suspected ability of the lipidation to stabilize secondary structure in a non-covalent manner that is analogous to what the lactam bond provides. One last change was the inversion of serine stereochemistry (d-Ser) at position two in order to render the analog resistant to dipeptidyl peptidase IV (DPP-IV)-mediated degradation, which is the endogenous enzyme responsible for N-terminal truncation of the first two amino acids of GLP-1, GIP, and glucagon. Secondly, this substitution at position two

also serves to preserve the potency at GcgR. This single peptide (Table 1, peptide 10) had a receptor activity profile similar to the starting peptide, but did not install any appreciable gain in GIPR agonism.

We had previously observed that enhanced alpha helical content is beneficial for inducing mixed agonism of GLP-1R and GcgR[1]. To determine if enhancing helicity likewise imparts GIPR agonism, further stabilization of the backbone helix within the aforementioned lipidated peptide (Table 1, peptide 10) was achieved with employment of an aminoisobutyric acid (Aib) substitution at position 16. Additionally and with the eventual intent for using these compounds *in vivo*, Aib was also employed at position two in order to convey resistance to DPP-IV inactivation in an analogous fashion as d-Ser. We have previously observed that $Aib^2$ also contributes to mixed agonism at GLP-1R and GIPR[2], however this substitution can be detrimental to glucagon activity. Therefore, a series of glucagon-specific residues were introduced to counter-act this anticipated loss in GcgR potency, which included $Arg^{17}$, $Gln^{20}$, and $Asp^{28}$, of which the latter substitution also enhances aqueous solubility in neutral pH buffers[7]. However, these cumulative substitutions (Table 1, peptide 11), despite preserving GcgR potency, did not introduce appreciable GIP activity when compared to the initial lipidated analog (Table 1, peptide 11).

In a parallel modification to the lipidated analog (Table 1, peptide 10), we included $Aib^2$, but we retained $Glu^{16}$ instead of substitution with $Aib^{16}$. $Glu^{16}$ likewise stabilizes the alpha helix through a non-covalent intra-helical interaction with $Lys^{20}$ albeit to a lesser degree than $Aib^{16}$, as in **peptide 11**. $Glu^{16}$ also provokes mixed agonism at GLP-1R and GcgR, and was thus retained to counterbalance the detrimental effects of $Aib^2$ on GcgR activity. We also included $Leu^{27}$, which is specific to native glucagon, in an additional attempt to boost glucagon activity. But

again much like the aforementioned previous attempts, these cumulative substitutions failed to enhance GIPR activity despite enhancing balanced, mixed agonism at GLP-1R and GcgR (Table 1, peptide 12). Each of these separate yet collective changes highlighted in **peptide 11** and **peptide 12** was investigated as a means to retain glucagon potency yet enhance GIP potency. Despite these failures in gaining GIP activity, these modifications led to the discovery of a high potency GLP-1/glucagon co-agonist with lipidation suitable for use *in vivo* and of enhanced solubility and chemical stability relative to the native hormones (Table 1, peptide 12). Nonetheless, the primary objective of balanced tri-agonism was no closer to a reality than when we started since **peptide 12** is reduced in GIP potency relative to the other two constituent activities by approximately one thousand-fold.

The structure-activity relationship (SAR) of position 2 was interrogated as we have previously reported the constructive interactions at this site with the central region of the peptide to change bioactivity[8]. To make a peptide backbone suitable for position 2 SAR without a subsequent loss of glucagon potency, a peptide scaffold was generated using several of the previously employed changes in the middle and C-terminal regions of **peptide 11** and **peptide 12**, including $Glu^{16}$, $Arg^{17}$, $Gln^{20}$, $Leu^{27}$, and $Asp^{28}$, all of which also serve auxiliary functions to enhance solubility and chemical stability. Additionally, in an attempt to selectively enhance GIP and glucagon activity, we introduced $Asp^{21}$ and $Val^{23}$, which are each specific to native GIP and glucagon. Mixed agonism at GLP-1R and GcgR was preserved without an enrichment of agonism at GIPR (Table 1, peptide 13). Since the second amino acid influences selective activity at each constitutive receptor target, and also because the residues in the native sequences of GLP-1, GIP, and glucagon (alanine and serine) are both susceptible to *in vivo* proteolysis by DPP-IV[9,10], we chose amino acid

substitutions that retain a slightly different side chain composition, but one that was resistant to enzymatic cleavage. However, substitution with $Aib^2$, $dSer^2$, $Gly^2$, sarcosine ($Sar^2$), or $dAla^2$ did not appreciably change any of the constitutive receptor activity profiles (Table 1, peptides 13-17) such that unimolecular tri-agonism still remained elusive.

In discovering the dual GLP-1/GIP co-agonist, we observed that the terminal ends of the peptide need to be coordinately optimized to achieve high potency dual incretin receptor agonism[2]. Consequently, we inserted the three C-terminal residues of one of the endogenous forms of GLP-1, which included $Gly^{29}$, $Arg^{30}$, and $Gly^{31}$, into the $dSer^2$ containing **peptide 14** to generate an analog of 31-amino acid length (Table 1, peptide 18). These elongating substitutions impart a subtle gain in GIP activity that inspired further C-terminal extension of the peptide. Application of the C-terminal-extended (Cex) residues from exendin-4 to generate a 39-residue analog (Table 1, peptide 19) resulted in enhanced GIP activity and represents a breakthrough in the SAR to realize substantially higher GIP potency than the starting point peptide, or any of the aforementioned intermediate analogs. However, the GIP activity in **peptide 19** was unbalanced relative to its GLP-1 and glucagon counterparts, with an $EC_{50}$ at GIPR that is of ~30-fold less relative potency (Table 1, peptide 19). Substitution with $Aib^2$ corrected this relative GIP imbalance to provide a unimolecular analog with a length identical to exendin-4, that is of exquisite potency and balance at each of the three receptors (Table 1, peptide 20). This peptide represents the first highly potent, balanced unimolecular triple agonist at GLP-1R, GIPR, and GcgR. Furthermore, this single molecule hybrid also possesses optimized chemical stability and pharmacokinetics due to site-specific acylation.

## References


1 Day, J. W. *et al.* A new glucagon and GLP-1 co-agonist eliminates obesity in rodents. *Nature chemical biology* **5**, 749-757, doi:10.1038/nchembio.209 (2009).

2 Finan, B. *et al.* Unimolecular dual incretins maximize metabolic benefits in rodents, monkeys, and humans. *Science translational medicine* **5**, 209ra151, doi:10.1126/scitranslmed.3007218 (2013).

3 Moon, M. J. *et al.* Tyr1 and Ile7 of glucose-dependent insulinotropic polypeptide (GIP) confer differential ligand selectivity toward GIP and glucagon-like peptide-1 receptors. *Molecules and cells* **30**, 149-154, doi:10.1007/s10059-010-0100-5 (2010).

4 Runge, S., Wulff, B. S., Madsen, K., Brauner-Osborne, H. & Knudsen, L. B. Different domains of the glucagon and glucagon-like peptide-1 receptors provide the critical determinants of ligand selectivity. *British journal of pharmacology* **138**, 787-794, doi:10.1038/sj.bjp.0705120 (2003).

5 Pocai, A. *et al.* Glucagon-like peptide 1/glucagon receptor dual agonism reverses obesity in mice. *Diabetes* **58**, 2258-2266, doi:10.2337/db09-0278 (2009).

6 Ward, B., Ottaway N., Perez-Tilve D., Ma D., Gelfanov VM.,Tschop MH., and DiMarchi RD. Structural Changes Associated with Peptide Lipidation Broaden Biological Function. *Molecular metabolism*, doi:10.1016/j.molmet.2013.08.008 (2013).

7 Chabenne, J. R., DiMarchi, M. A., Gelfanov, V. M. & DiMarchi, R. D. Optimization of the native glucagon sequence for medicinal purposes. *Journal of diabetes science and technology* **4**, 1322-1331 (2010).

8 Patterson, J. T., Day, J. W., Gelfanov, V. M. & DiMarchi, R. D. Functional association of the N-terminal residues with the central region in glucagon-related peptides. *Journal of peptide science : an official publication of the European Peptide Society* **17**, 659-666, doi:10.1002/psc.1385 (2011).

9 Pospisilik, J. A. *et al.* Metabolism of glucagon by dipeptidyl peptidase IV (CD26). *Regulatory peptides* **96**, 133-141 (2001).

10 Kieffer, T. J., McIntosh, C. H. & Pederson, R. A. Degradation of glucose-dependent insulinotropic polypeptide and truncated glucagon-like peptide 1 in vitro and in vivo by dipeptidyl peptidase IV. *Endocrinology* **136**, 3585-3596 (1995).

| Peptide # | Analog | GLP-1 Receptor | | | GIP Receptor | | | Glucagon Receptor | | |
|---|---|---|---|---|---|---|---|---|---|---|
| | | $EC_{50}$ (nM) | STDev | Relative % | $EC_{50}$ (nM) | STDev | Relative % | $EC_{50}$ (nM) | STDev | Relative % |
| 1 | GLP-1 | 0.028 | 0.002 | 100 | 1513.825 | 78.950 | 0 | 2449.288 | 106.460 | 0 |
| 2 | GLP-1 ($Aib^2$ $E^{16}$ Cex $K^{40}$-C16 acyl) **"Acyl-GLP-1"** | 0.015 | 0.001 | 187 | 122.883 | 10.668 | 0 | 162.402 | 29.771 | 0 |
| 3 | GIP | 1567.012 | 65.780 | 0 | 0.020 | 0.004 | 100 | 417.480 | 10.370 | 0 |
| 4 | GIP ($Aib^2$ Cex $K^{40}$-$C_{16}$ acyl) **"Acyl-GIP"** | 6.330 | 2.690 | 0 | 0.012 | 0.001 | 168 | 2.920 | 0.840 | 1 |
| 5 | Glucagon | 3.100 | 0.494 | 1 | 1538.109 | 329.020 | 0 | 0.032 | 0.006 | 100 |
| 6 | Glucagon ($Aib^2$ $K^{10}$-γEγE-$C_{16}$ acyl $Aib^{20}$) **"Acyl-glucagon"** | 0.479 | 0.068 | 6 | 22.650 | 6.100 | 0 | 0.005 | 0.001 | 625 |
| 7 | **"GLP-1/GIP co-agonist"** | 0.005 | 0.001 | 516 | 0.003 | 0.001 | 691 | 1.286 | 0.103 | 2 |
| GIP SAR | | | | | | | | | | |
| 8 | Glucagon ($E^{16}$ $Q^{17}$ $A^{18}$ $K^{20}$ $E^{21}$ $I^{23}$ $A^{24}$)-$NH_2$ | 0.022 | 0.002 | 127 | 6.258 | 1.278 | 0 | 0.031 | 0.009 | 103 |
| 9 | Peptide 8 ($E^3$)-$NH_2$ | 0.030 | 0.003 | 93 | 0.867 | 0.099 | 2 | 5.225 | 0.441 | 1 |
| 10 | Peptide 8 ($dS^2$ $K^{10}$-γE-C16 acyl)-$NH_2$ | 0.039 | 0.005 | 72 | 2.691 | 0.416 | 1 | 0.041 | 0.002 | 78 |
| 11 | Peptide 10 ($Aib^2$ $Aib^{16}$ $R^{17}$ $Q^{20}$ $D^{21}$ $Q^{24}$ $D^{28}$)-$NH_2$ | 0.015 | 0.003 | 187 | 2.194 | 0.329 | 1 | 0.028 | 0.009 | 114 |
| 12 | Peptide 10 ($Aib^2$ $E^{16}$ $L^{27}$ $D^{28}$)-$NH_2$ | 0.003 | 0.001 | 933 | 3.545 | 0.156 | 1 | 0.003 | 0.001 | 1067 |
| Position 2 SAR | | | | | | | | | | |
| 13 | Peptide 10 ($Aib^2$ $R^{17}$ $Q^{20}$ $D^{21}$ $V^{23}$ $Q^{24}$ $L^{27}$ $D^{28}$)-$NH_2$ | 0.068 | 0.008 | 41 | 2.032 | 0.117 | 1 | 0.005 | 0.001 | 640 |
| 14 | Peptide 13 ($dS^2$)-$NH_2$ | 0.003 | 0.001 | 933 | 1.654 | 0.164 | 1 | 0.006 | 0.001 | 533 |
| 15 | Peptide 13 ($G^2$)-$NH_2$ | 0.093 | 0.013 | 30 | 1.103 | 0.200 | 2 | 0.005 | 0.001 | 640 |
| 16 | Peptide 13 ($Sar^2$)-$NH_2$ | 0.115 | 0.014 | 24 | 5.828 | 0.334 | 0 | 0.016 | 0.003 | 200 |
| 17 | Peptide 13 ($dA^2$)-$NH_2$ | 0.040 | 0.005 | 70 | 1.646 | 0.298 | 1 | 0.009 | 0.001 | 356 |
| 18 | Peptide 14 ($G^{29}$ $R^{30}$ $G^{31}$)-$NH_2$ | 0.002 | 0.001 | 1400 | 0.812 | 0.101 | 2 | 0.004 | 0.001 | 800 |
| 19 | Peptide 14 ($G^{29}$ Cex)-$NH_2$ | 0.002 | 0.001 | 1400 | 0.085 | 0.009 | 24 | 0.003 | 0.001 | 1067 |
| 20 | Peptide 19 ($Aib^2$)-$NH_2$ **"Tri-agonist"** | 0.003 | 0.001 | 933 | 0.003 | 0.001 | 673 | 0.004 | 0.001 | 800 |
| Position 3 SAR | | | | | | | | | | |
| 21 | Peptide 20 ($hSer^3$)-$NH_2$ | 0.003 | 0.001 | 933 | 0.004 | 0.001 | 505 | 0.016 | 0.002 | 200 |
| 22 | Peptide 20 ($nVal^3$)-$NH_2$ | 0.003 | 0.001 | 933 | 0.002 | 0.001 | 1010 | 0.025 | 0.004 | 128 |
| 23 | Peptide 20 ($V^3$)-$NH_2$ | 0.006 | 0.001 | 467 | 0.005 | 0.001 | 404 | 0.026 | 0.004 | 123 |
| 24 | Peptide 20 ($nLeu^3$)-$NH_2$ | 0.003 | 0.001 | 933 | 0.003 | 0.001 | 673 | 0.033 | 0.003 | 97 |
| 25 | Peptide 20 ($Dap(Ac)^3$)-$NH_2$ | 0.002 | 0.001 | 1400 | 0.010 | 0.002 | 202 | 0.043 | 0.006 | 74 |
| 26 | Peptide 20 ($Met(O)^3$)-$NH_2$ **"Imbalanced tri-agonist"** | 0.003 | 0.001 | 933 | 0.018 | 0.002 | 112 | 0.089 | 0.007 | 36 |
| 27 | Peptide 20 ($E^3$)-$NH_2$ **"Matched co-agonist"** | 0.004 | 0.001 | 700 | 0.002 | 0.001 | 1010 | 1.420 | 0.090 | 2 |
| FLATT | | | | | | | | | | |
| 28 | **YAG-Glucagon** | 5.484 | 0.423* | 1 | 1128.970 | 57.430* | 0 | 3.270 | 0.109* | 1 |
| 29 | **[$DA^2$]GLP-1/GcG** | 100.480 | 0.411* | 0 | 17.110 | 0.920* | 0 | 5.139 | 0.184* | 1 |
| RECIPROCAL | | | | | | | | | | |
| 30 | **GLP-1/glucagon** | 0.004 | 0.001 | 700 | 0.133 | 0.084 | 15 | 0.007 | 0.002 | 457 |
| 31 | **GIP/glucagon** | 0.568 | 0.192 | 5 | 0.004 | 0.001 | 505 | 0.008 | 0.003 | 400 |

**Supplementary Table 1. *In vitro* human receptor activity profile of peptides.** $EC_{50}$ values represent the effective peptide concentrations (nM) that stimulate half-maximal activation at the human GLP-1, GIP, and glucagon receptors. STDev values represent the standard deviation of the calculated $EC_{50}$ from each separate experiment. A minimum of three separate experiments was performed for each peptide at each respective receptor. Those peptides denoted with an asterisk (*) were only tested once at each respective receptor. Relative % activity at each receptor = (native ligand $EC_{50}$/analog $EC_{50}$) x 100. Continuing down from peptide 10, the peptides feature the same sequence of the peptide number denoted in the analog box with the subsequent modification contained within the parentheses. All sequences are found in Supplementary Figure 1.

| Peptide # | Analog Name | Theoretical Mass | Observed Mass |
|---|---|---|---|
| 1 | GLP-1 | 3355.71 | 3357.1 |
| 2 | GLP-1 ($Aib^2$ $E^{16}$ Cex $K^{40}$-C16 acyl) **"Acyl-GLP-1"** | 4429.06 | 4429.72 |
| 3 | GIP | 4855.46 | 4856.00 |
| 4 | GIP ($Aib^2$ Cex $K^{40}$-$C_{16}$ acyl) **"Acyl-GIP"** | 4606.28 | 4606.37 |
| 5 | Glucagon | 3482.79 | 3483.40 |
| 6 | Glucagon ($Aib^2$ $K^{10}$-γEγE-$C_{16}$ acyl $Aib^{20}$) **"Acyl-glucagon"** | 3868.42 | 3868.49 |
| 7 | **"GLP-1/GIP co-agonist"** | 4473.11 | 4473.14 |
| GIP SAR | | | |
| 8 | Glucagon ($E^{16}$ $Q^{17}$ $A^{18}$ $K^{20}$ $E^{21}$ $I^{23}$ $A^{24}$)-$NH_2$ | 3381.73 | 3382.19 |
| 9 | Peptide 8 ($E^3$)-$NH_2$ | 3383.69 | 3384.10 |
| 10 | Peptide 8 ($dS^2$ $K^{10}$-γE-C16 acyl)-$NH_2$ | 3714.25 | 3713.00 |
| 11 | Peptide 10 ($Aib^2$ $Aib^{16}$ $R^{17}$ $Q^{20}$ $D^{21}$ $Q^{24}$ $D^{28}$)-$NH_2$ | 3726.27 | 3727.40 |
| 12 | Peptide 10 ($Aib^2$ $E^{16}$ $L^{27}$ $D^{28}$)-$NH_2$ | 3695.23 | 3694.50 |
| Position 2 SAR | | | |
| 13 | Peptide 10 ($Aib^2$ $R^{17}$ $Q^{20}$ $D^{21}$ $V^{23}$ $Q^{24}$ $L^{27}$ $D^{28}$)-$NH_2$ | 3727.25 | 3726.00 |
| 14 | Peptide 13 ($dS^2$)-$NH_2$ | 3754.22 | 3753.00 |
| 15 | Peptide 13 ($G^2$)-$NH_2$ | 3721.90 | 3720.50 |
| 16 | Peptide 13 ($Sar^2$)-$NH_2$ | 3735.91 | 3735.00 |
| 17 | Peptide 13 ($dA^2$)-$NH_2$ | 3738.22 | 3738.00 |
| 18 | Peptide 14 ($G^{29}$ $R^{30}$ $G^{31}$)-$NH_2$ | 3924.39 | 3924.16 |
| 19 | Peptide 14 ($G^{29}$ Cex)-$NH_2$ | 4546.03 | 4546.00 |
| 20 | Peptide 19 ($Aib^2$)-$NH_2$ **"Tri-agonist"** | 4543.08 | 4544.26 |
| Position 3 SAR | | | |
| 21 | Peptide 20 ($hSer^3$)-$NH_2$ | 4516.05 | 4515.50 |
| 22 | Peptide 20 ($nVal^3$)-$NH_2$ | 4528.11 | 4530.80 |
| 23 | Peptide 20 ($V^3$)-$NH_2$ | 4528.11 | 4529.60 |
| 24 | Peptide 20 ($nLeu^3$)-$NH_2$ | 4528.11 | 4528.00 |
| 25 | Peptide 20 ($Dap(Ac)^3$)-$NH_2$ | 4543.08 | 4543.00 |
| 26 | Peptide 20 ($Met(O)^3$)-$NH_2$ **"Imbalanced tri-agonist"** | 4576.17 | 4577.47 |
| 27 | Peptide 20 ($E^3$)-$NH_2$ **"Matched co-agonist"** | 4544.06 | 4545.05 |
| FLATT | | | |
| 28 | **YAG-Glucagon** | 3259.54 | 3259.56 |
| 29 | **[$DA^2$]GLP-1/GcG** | 3556.01 | 3556.03 |
| RECIPROCAL | | | |
| 30 | **GLP-1/glucagon** | 3921.43 | 3922.39 |
| 31 | **GIP/glucagon** | 4484.18 | 4484.00 |

**Supplementary Table 2. Mass profiles for peptide analogs.** Theoretical and observed masses of each analog. Peptide molecular weights were determined electrospray ionization (ESI) or matrix-assisted laser desorption/ionization time-of-flight (MALDI-TOF) mass spectrometry, and character was confirmed by analytical reversed-phase high performance liquid chromatography (HPLC).

| Species | Peptide | GLP1R | | GIPR | | GCGR | |
|---|---|---|---|---|---|---|---|
| | | $EC_{50}$ [nM] | | $EC_{50}$ [nM] | | $EC_{50}$ [nM] | |
| | | Mean | SD | Mean | SD | Mean | SD |
| Mouse | **GLP-1/GIP co-agonist** | 0.280 | 0.030 | 0.071 | 0.020 | 10.100 | 1.830 |
| | **Tri-agonist (peptide 20)** | 0.070 | 0.030 | 0.060 | 0.020 | 0.040 | 0.020 |
| | **Native Ligand** | 0.080 | 0.005 | 0.050 | 0.010 | 0.008 | 0.004 |
| | | | | | | | |
| Rat | **GLP-1/GIP co-agonist** | 0.124 | 0.080 | 0.040 | 0.016 | 20.317 | 11.390 |
| | **Tri-agonist (peptide 20)** | 0.060 | 0.030 | 0.030 | 0.010 | 0.090 | 0.030 |
| | **Native Ligand** | 0.050 | 0.005 | 0.010 | 0.007 | 0.032 | 0.016 |
| | | | | | | | |
| Cyno | **GLP-1/GIP co-agonist** | 0.117 | 0.070 | 0.109 | 0.105 | 28.585 | 2.425 |
| | **Tri-agonist (peptide 20)** | 0.060 | 0.010 | 0.080 | 0.030 | 0.090 | 0.020 |
| | **Native Ligand** | 0.080 | 0.040 | 0.030 | 0.010 | 0.190 | 0.030 |

**Supplementary Table 3. cAMP production in CHO cells individually expressing recombinant mouse-, rat-, or cynomolgus monkey-derived GLP-1R, GIPR, or GcgR.** $EC_{50}$ values represent the effective peptide concentrations (nM) that stimulate half-maximal activation, as assessed by cAMP accumulation, at the mouse, rat, and cyno GLP-1, GIP, and glucagon receptors. SD values represent the standard deviation of the calculated $EC_{50}$ from each separate experiment. A minimum of three separate experiments was performed for each peptide at each respective receptor from each species.

| Receptor | Non-Specific Ligand | Radioligand | Cell Souce | Receptor Source | Incubation Time (min) | Incubation Temp (°C) | Specific Binding % | STDev | % Inhibition of Control |
|---|---|---|---|---|---|---|---|---|---|
| A1 Adenosine Receptor | DPCPX (1μM) | DPCPX (1nM) | CHO | Recombinant | 60 | RT | 96.3 | 5.7 | 3.8 |
| A2A Adenosine Receptor | NECA (10μM) | CGS (6nM) | HEK-293 | Recombinant | 120 | RT | 112.2 | 11.2 | -12.2 |
| A3 Adenosine Receptor | IB-MECA (1μM) | IB-MECA (0.15nM) | HEK-293 | Recombinant | 120 | RT | 127.2 | 7.7 | -27.2 |
| Alpha 1 Adrenergic Receptor | Prazosin (0.5μM) | Prazosin (0.25nM) | Rat Cortex | Endogenous | 60 | RT | 105.7 | 2.5 | -5.7 |
| Alpha 2 Adrenergic Receptor | (-) Epinepherine (100μM) | RX 8211002 (0.5nM) | Rat Cortex | Endogenous | 60 | RT | 109.1 | 28.6 | -9.1 |
| Beta 1 Adrenergic Receptor | Alprenolol (50μM) | CGP 12177 (0.3nM) | HEK-293 | Recombinant | 60 | RT | 92.6 | 8.4 | 7.5 |
| Beta 2 Adrenergic Receptor | Alprenolol (50μM) | CGP 12177 (0.3nM) | CHO | Recombinant | 120 | RT | 106.3 | 5.6 | -6.3 |
| Norepinepherine Transporter | Desipramine (1μM) | Nisoxetine (1nM) | CHO | Recombinant | 120 | 4 | 111.5 | 6.3 | -11.5 |
| Angiotensin II Receptor Type 1 | Angiotensin II (10μM) | $Sar^1$, $Ile^4$-Angiotensin II (0.05nM) | HEK-293 | Recombinant | 120 | 37 | 135.2 | 9.1 | -35.2 |
| Angiotensin II Receptor Type 2 | Angiotensin II (10μM) | CGP 42112A (0.01nM) | HEK-293 | Recombinant | 240 | 37 | 101.0 | 5.2 | -0.9 |
| Central Benzodiazepine Receptor | Diazepam (3μM) | Flunitrazepam (0.4nM) | Rat Cortex | Endogenous | 60 | 4 | 124.9 | 8.7 | -24.9 |
| Peripheral Benzodiazepine Receptor | PK 11195 (10μM) | PK 11195 (0.2nM) | Rat Heart | Endogenous | 15 | RT | 108.1 | 7.7 | -8.1 |
| Bombesin Receptor | Bombesin (1μM) | $Tyr^4$-Bombesin (0.01nM) | Rat Cortex | Endogenous | 60 | RT | 105.2 | 1.7 | -5.2 |
| Bradykinin Receptor B2 | Bradykinin (1μM) | Bradykinin (0.3nM) | CHO | Recombinant | 60 | RT | 101.6 | 3.9 | -1.6 |
| Calcitonin Receptor-Like Receptor | CGRPa (1μM) | CGRPa (0.03nM) | CHO | Recombinant | 90 | RT | 112.5 | 9.3 | -12.5 |
| L-Type Calcium Channel | D 600 (10μM) | D 888 (3nM) | Rat Cortex | Endogenous | 120 | RT | 117.8 | 0.7 | -17.8 |
| Small Conductance Calcium-Activated Potassium Channel | Apamin (100nM) | Apamin (0.007nM) | Rat Cortex | Endogenous | 60 | 4 | 98.2 | 11.2 | 1.8 |
| Cannabinoid Receptor Type 1 | WIN 552312-2 (10μM) | CP559400.5nM) | CHO | Recombinant | 120 | 37 | 111.4 | 6.4 | -11.4 |
| Cholecystokinin A Receptor | CCK (1μM) | CCK (0.08nM) | CHO | Recombinant | 60 | RT | 111.9 | 4.8 | -11.9 |
| Cholecystokinin B Receptor | CCK (1μM) | CCK (0.08nM) | CHO | Recombinant | 60 | RT | 120.4 | 9.3 | -20.4 |
| Dopamine Receptor D1 | SCH 23390 (1μM) | SCH 23390 (0.3nM) | CHO | Recombinant | 60 | RT | 111.2 | 0.4 | -11.2 |
| Dopamine Receptor D2 | (+) Butaclamol (10μM) | Methyl-spiperone (0.3nM) | HEK-293 | Recombinant | 60 | RT | 94.0 | 3.1 | 6.0 |
| Dopamine Receptor D3 | (+) Butaclamol (10μM) | Methyl-spiperone (0.3nM) | CHO | Recombinant | 60 | RT | 113.8 | 4.9 | -13.8 |
| Dopamine Receptor D4 | (+) Butaclamol (10μM) | Methyl-spiperone (0.3nM) | CHO | Recombinant | 60 | RT | 110.0 | 6.8 | -10.0 |
| Dopamine Receptor D5 | SCH 23390 (10μM) | SCH 23390 (0.3nM) | GH4 | Recombinant | 60 | RT | 109.1 | 8.1 | -9.1 |
| Endothelin Receptor Type A | Endothelin-1 (100μM) | Endothelin-1 (0.03nM) | CHO | Recombinant | 120 | 37 | 117.3 | 12.0 | -17.3 |
| Endothelin Receptor Type B | Endothelin-1 (0.1μM) | Endothelin-1 (0.03nM) | CHO | Recombinant | 120 | 37 | 103.0 | 12.3 | -3.0 |
| Dopamine Transporter | BTCP (10μM) | BTCP (4.5nM) | CHO | Recombinant | 120 | 4 | 103.1 | 0.6 | -3.1 |
| GABA Receptor | GABA (100μM) | GABA (10nM) | Rat Cortex | Endogenous | 60 | RT | 103.5 | 6.6 | -3.5 |
| GABA-Gated Chloride Channel | Picrotoxinin (20μM) | TBPS (3nM) | Rat Cortex | Endogenous | 120 | RT | 94.3 | 4.5 | 5.8 |
| Galanin Receptor 1 | Galanin (1μM) | Galanin (0.1nM) | HEK-293 | Recombinant | 60 | RT | 115.6 | 3.5 | -15.6 |
| Galanin Receptor 2 | Galanin (1μM) | Galanin (0.05nM) | CHO | Recombinant | 120 | RT | 99.8 | 1.8 | 0.2 |
| Glucocorticoid Receptor | Triamcinolone (10μM) | Dexamethasone (1.5nM) | IM-9 | Endogenous | 360 | 4 | 100.5 | 3.1 | -0.5 |
| Glucagon Receptor | Glucagon (1μM) | Glucagon (0.025nM) | CHO | Recombinant | 120 | RT | 23.3 | 5.9 | 76.7 |
| Glucagon-Like Peptide 1 Receptor | GLP-1 (1μM) | GLP-1 (0.025nM) | BTC6 | Endogenous | 120 | 37 | -5.6 | 4.7 | 105.6 |
| Platelet-Derived Growth Factor Receptor | PDGF BB (10nM) | PDGF (0.3nM) | Balb/c 3T3 | Endogenous | 180 | 4 | 104.8 | 1.7 | -4.8 |
| Interleukin 8 Receptor | IL-8 (30nM) | IL-8 (0.025nM) | HEK-293 | Recombinant | 60 | RT | 101.3 | 0.0 | -1.3 |
| C-C Chemokine Receptor Type 1 | MIP-1a (100nM) | MIP-1a (0.01nM) | HEK-293 | Recombinant | 120 | RT | 109.7 | 6.0 | -9.7 |
| Cluster of Differentiation 120 | TNFa (10nM) | TNFa (0.1nM) | U-937 | Endogenous | 120 | 4 | 102.2 | 2.3 | -2.2 |
| Histamine H1 Receptor | Pyrilamine (1μM) | Pyrilamine (1nM)) | HEK-293 | Recombinant | 60 | RT | 98.1 | 11.0 | 1.9 |
| Histamine H2 Receptor | Tiotidine (100μM) | APT (0.075nM) | CHO | Recombinant | 120 | RT | 120.4 | 7.1 | -20.4 |
| Melanocortin 4 Receptor | NDP-aMSH (1μM) | NDP-aMSH (0.05nM) | CHO | Recombinant | 120 | 37 | 109.0 | 3.3 | -8.9 |
| Melatonin Receptor Type 1A | Melatonin (1μM) | 2-Iodomelatonin (0.01nM) | CHO | Recombinant | 60 | RT | 113.3 | 8.1 | -13.3 |
| Muscarinic Acetylcholine Receptor M1 | Atropine (1μM) | Pirenzepine (2nM) | CHO | Recombinant | 60 | RT | 133.1 | 5.0 | -33.1 |
| Muscarinic Acetylcholine Receptor M2 | Atropine (1μM) | AF-DX 384 (2nM) | CHO | Recombinant | 60 | RT | 110.1 | 6.2 | -10.1 |
| Muscarinic Acetylcholine Receptor M3 | Atropine (1μM) | 4-DAMP (0.2nM) | CHO | Recombinant | 60 | RT | 103.2 | 3.8 | -3.2 |
| Muscarinic Acetylcholine Receptor M4 | Atropine (1μM) | 4-DAMP (0.2nM) | CHO | Recombinant | 60 | RT | 117.7 | 13.1 | -17.7 |
| Muscarinic Acetylcholine Receptor M5 | Atropine (1μM) | 4-DAMP (0.3nM) | CHO | Recombinant | 60 | RT | 108.7 | 8.2 | -8.7 |
| Tachykinin Receptor NK1 | $Sar^1$, $Met(O^2)^{11}$-Substance P (1μM) | BH-Substance P (0.15nM) | U-373MG | Endogenous | 60 | RT | 105.4 | 0.8 | -5.4 |
| Tachykinin Receptor NK2 | $Nleu^{10}$-Neurokinin A (4-10) (300nM) | Neurokinin A (0.1nM) | CHO | Recombinant | 60 | RT | 108.4 | 10.2 | -8.4 |
| Tachykinin Receptor NK3 | SB 222200 (10μM) | SR 142801 (0.4nM) | CHO | Recombinant | 120 | RT | 105.6 | 4.5 | -5.6 |
| Neuropeptide Y Receptor Y1 | NPY (1μM) | Peptide YY (0.025nM) | SK-N-MC | Endogenous | 120 | 37 | 103.6 | 1.1 | -3.6 |
| Neuropeptide Y Receptor Y2 | NPY (1μM) | Peptide YY (0.015nM) | KAN-TS | Endogenous | 60 | 37 | 113.3 | 7.1 | -13.3 |
| Neurotensin Receptor 1 | Neurotensin (1μM) | $Tyr^3$-Neurotensin (0.05nM) | CHO | Recombinant | 60 | 4 | 108.5 | 1.7 | -8.5 |
| N-Methyl-D-Aspartate Receptor | MK 801 (10μM) | TCP (10nM) | Rat Cortex | Endogenous | 120 | 37 | 103.0 | 10.0 | -3.0 |
| Delta Opioid Receptor | Naltrexone (10μM) | DADLE (0.5nM) | CHO | Recombinant | 120 | RT | 101.0 | 2.6 | -0.9 |
| Kappa Opioid Receptor | Naloxone (10μM) | U 69593 (1nM) | CHO | Recombinant | 60 | RT | 109.2 | 8.1 | -9.2 |
| Mu Opioid Receptor | Naloxone (10μM) | DAMGO (0.5nM) | HEK-293 | Recombinant | 120 | RT | 100.4 | 5.0 | -0.3 |
| Nociceptin Receptor | Nociceptin (1μM) | Nociceptin (0.2nM) | HEK-293 | Recombinant | 60 | RT | 99.7 | 1.8 | 0.3 |
| Pituitary Adenylate Cyclase-Activating Polypeptide Type 1 Receptor | PACAP (1-27) (100nM) | PACAP (1-27) (100nM) | CHO | Recombinant | 120 | RT | 112.8 | 7.6 | -12.8 |
| Peroxisome Proliferator-Activated Receptor Gamma | Rosiglitazone (10μM) | Rosiglitazone (5nM) | E. coli | Recombinant | 120 | 4 | 94.5 | 7.1 | 5.6 |
| Voltage-Gated Potassium Channel | a-Dendrotoxin (50nM) | a-Dendrotoxin (0.01nM) | Rat Cortex | Endogenous | 60 | RT | 112.2 | 1.0 | -12.2 |
| Prostaglandin E2 Receptor | $PGE_2$ (10μM) | $PGE_2$ (3nM) | HEK-293 | Recombinant | 120 | RT | 102.7 | 8.5 | -2.7 |
| Prostaglandin E4 Receptor | PGE2 (10μM) | $PGE_2$ (0.5nM) | HEK-293 | Recombinant | 120 | RT | 106.1 | 0.6 | -6.1 |
| Prostacyclin Receptor | Iloprost (10μM) | Iloprost (6nM) | HEK-293 | Recombinant | 60 | RT | 118.2 | 9.3 | -18.2 |
| Purinergic Receptor | dATPaS (10μM) | dATPaS (10nM) | Rat Cortex | Endogenous | 60 | RT | 91.2 | 5.2 | 8.8 |
| Purinergic Receptor P2X | a,B-MeATP (10μM) | a,B-MeATP (3nM) | Rat Bladder | Endogenous | 120 | 4 | 101.6 | 0.9 | -1.6 |
| Serotonin Receptor $HT_{1A}$ | 8-OH-DPAT (10μM) | 8-OH-DPAT (0.3nM) | HEK-293 | Recombinant | 60 | RT | 106.7 | 0.3 | -6.7 |
| Serotonin Receptor $HT_{1B}$ | Serotonin (10μM) | CYP (0.1nM) / isoproterenol (30μM) | Rat Cortex | Endogenous | 120 | 37 | 107.8 | 10.1 | -7.7 |
| Serotonin Receptor $HT_{2A}$ | Ketanserin (1μM) | Ketanserin (0.5nM) | HEK-293 | Recombinant | 60 | RT | 104.5 | 4.7 | -4.5 |
| Serotonin Receptor $HT_{2B}$ | (±) DOI (1μM) | (±) DOI (0.2nM) | CHO | Recombinant | 60 | RT | 109.9 | 11.6 | -9.9 |
| Serotonin Receptor $HT_{2C}$ | RS 102221 (10μM) | Mesulergine (1nM) | HEK-293 | Recombinant | 120 | 37 | 104.4 | 4.0 | -4.3 |
| Serotonin Receptor $HT_3$ | MDL 72222 (10μM) | BRL 43694 (0.5nM) | CHO | Recombinant | 120 | RT | 100.7 | 1.8 | -0.7 |
| Serotonin Receptor $HT_{5A}$ | Serotonin (100μM) | LSD (1.5nM) | HEK-293 | Recombinant | 120 | 37 | 102.3 | 3.1 | -2.3 |
| Serotonin Receptor $HT_6$ | Serotonin (100μM) | LSD (2nM) | CHO | Recombinant | 120 | 37 | 103.3 | 4.0 | -3.3 |
| Serotonin Receptor $HT_7$ | Serotonin (10μM) | LSD (4nM) | CHO | Recombinant | 120 | RT | 118.4 | 7.4 | -18.4 |
| Serotonin Transporter | Imipramine (10μM) | Imipramine (2nM) | CHO | Recombinant | 60 | RT | 109.1 | 6.6 | -9.1 |
| Sigma Receptor | Haloperidol (10μM) | DTG (10nM) | Jurkat | Endogenous | 120 | RT | 105.4 | 1.6 | -5.4 |
| Somatostatin Receptor | Somatostatin (300nM) | $Tyr^3$-Somatostatin (0.05nM) | AtT-20 | Endogenous | 60 | 37 | 111.3 | 10.0 | -11.3 |
| Vasoactive Intestinal Polypeptide Receptor 1 | VIP (1μM) | VIP (0.04nM) | CHO | Recombinant | 60 | RT | 94.8 | 0.6 | 5.3 |
| Arginine Vasopressin Receptor 1A | AVP (1μM) | AVP (0.3nM) | CHO | Recombinant | 60 | RT | 95.1 | 2.8 | 5.0 |

**Supplementary Table 4. *In vitro* receptor binding profile of the tri-agonist at off-target receptors.** The GLP-1/GP/glucagon tri-agonist was screened for non-selective binding at 79 receptors or ion channels using customized high-throughput competitive binding assays. Results are expressed as % specific binding, calculated by [(tri-agonist specific binding / control specific binding) x 100], and also as % inhibition of control, calculated by [100 – (tri-agonist specific binding / control specific binding) x 100]. In general, results showing a % inhibition of control that is greater than 25% is considered a positive result of specific receptor binding and values less than 25% are considered a negative result of specific receptor binding. For each individual assay at the respective receptors, the ligand used to measure non-specific binding, the radioligand utilized to measure displacement from the receptor, the source of the receptor, and assay conditions are listed in the table. The tri-agonist was tested at a concentration of 1 μM and the non-specific ligands and radioligands were tested at the concentrations depicted in the table. A minimum of two separate experiments was performed for each respective receptor.

Nature Medicine: doi:10.1038/nm.3761

| Cells | GLP-1 | GIP | Glucagon | GLP-1/GIP Co-agonist | Tri-agonist (Peptide 20) |
|---|---|---|---|---|---|
| MIN6 | 0.45 ± 0.09 | 16.87 ± 4.00 | 31.29 ± 7.33 | 1.13 ± 0.56 | 0.81 ± 0.08 |
| Rat hepatocytes | N/A | N/A | 0.65 ± 0.55 | 21.32 ± 8.97 | 0.59 ± 0.29 |
| 3T3-L1 adipocytes | N/A | 1.41 ± 0.30 | N/A | 0.53 ± 0.32 | 4.55 ± 5.61 |

**Supplementary Table 5. Effects of the tri-agonist on cAMP production in cultured pancreatic β cells, hepatocytes, and adipocytes.** Values represent mean $EC_{50}$ ± standard deviation (nM) of cAMP production in the respective cell lines in response to a 30 min stimulation with the indicated peptides. Human GLP-1, GIP, and glucagon were used. A minimum of three separate experiments was performed for each peptide in each cell line.

| **Tri-agonist / peptide 20** | Species | | | | |
|---|---|---|---|---|---|
| | C57BL/6J Mice | DIO Mice | Rats | Dogs | Monkeys |
| Dose (mg/kg) / (nmol/kg) | 0.045 / 10 | 0.045 / 10 | 0.045 / 10 | ND | 0.015 / 3 |
| $C_{max}$ (ng/ml) | 195 | 636 | 34 | ND | 112 |
| $t_{max}$ (h) | 4 | 2 | 2 | ND | 4 |
| $t_{1/2}$ (h) | ~5 | ~4 | ~6 | ND | ~5 |
| **GLP-1/GIP co-agonist** | Species | | | | |
| | C57BL/6J Mice | DIO Mice | Rats | Dogs | Monkeys |
| Dose (mg/kg) / (nmol/kg) | 0.15 / 3 | ND | 1 / 222 | 0.045 / 10 | 0.045 / 10 |
| $C_{max}$ (ng/ml) | 383 | ND | 480 | 90 | 55 |
| $t_{max}$ (h) | 4 | ND | 4 | 4 | 6 |
| $t_{1/2}$ (h) | ~12 | ND | ~8 | ~6 | ~5 |

**Supplementary Table 6. Pharmacokinetic comparison of the GLP-1/GIP co-agonist and the tri-agonist in different species.** The pharmacokinetic parameters of the tri-agonist and the dual incretin co-agonist were determined following a subcutaneous injection of the peptides at the indicated doses in the different species. The concentration of the peptides in plasma was determined by LC-MS/MS and the pharmacokinetic analyses were determined by non-compartmental analysis with WinNonLin. $C_{max}$, maximal plasma concentration; $t_{max}$, time for maximal concentration, $t_{1/2}$, elimination half-life.


**Supplementary Figure 1. Sequences of peptide analogs.** Amino acid sequences of intermediate peptide analogs with the iterative residue substitutions from the preceding analog highlighted in blue. Aminoisobutyric acid is denoted as X. Lysine with a γE-$C_{16}$ acyl attached through the side chain amine is denoted as underlined K. Sarcosine is denoted as #. D-enantiomers of select amino acids are italicized.

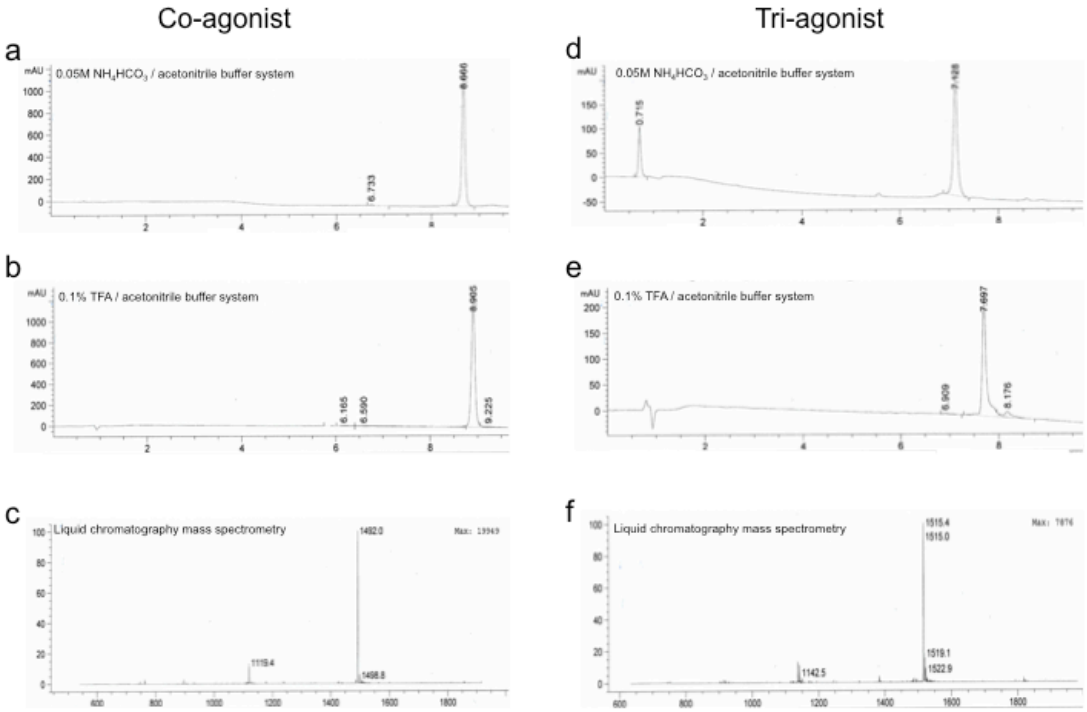


**Supplementary Figure 2. HPLC and mass spectrometry.** HPLC traces of the GLP-1/GIP co-agonist using a **(a)** basic buffer system and a **(b)** acidic buffer system. **(c)** LC-MS data of the GLP-1/GIP co-agonist. HPLC traces of the tri-agonist using a **(d)** basic buffer system and a **(e)** acidic buffer system. **(f)** LC-MS data of the tri-agonist.

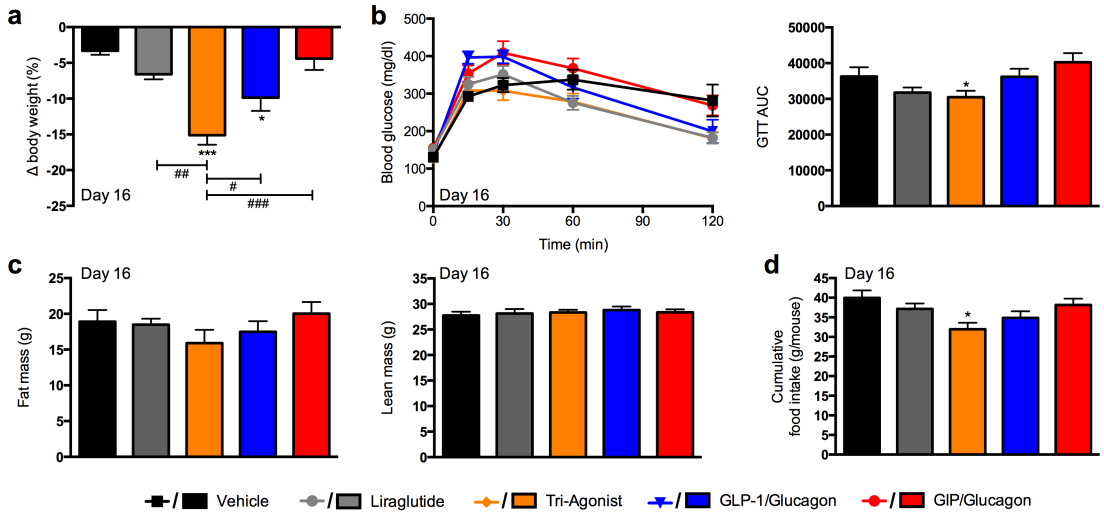


**Supplementary Figure 3. Comparison to the tri-agonist to GLP-1/ glucagon and GIP/glucagon co-agonists.** Effects on **(a)** body weight change, **(b)** glucose tolerance on day 16, **(c)** final body composition, and **(d)** cumulative food intake of male DIO mice treated with vehicle (black squares), liraglutide (gray circles), the GLP-1/GIP/glucagon tri-agonist (orange diamonds), a matched GLP-1/glucagon co-agonist (blue triangles), or a matched GIP/glucagon co-agonist (red circles). All mice were treated by daily subcutaneous injections at a dose of 3 nmoles $kg^{-1}$. Data in **(a–d)** represent means ± s.e.m. $^{*}P < 0.05$, $^{**}P < 0.01$, $^{***}P < 0.001$, determined by ANOVA comparing vehicle to compound injections, and $^{\#\#}P < 0.01$, $^{\#\#\#}P < 0.001$, determined ANOVA comparing tri-agonist injections to co-agonist injections. In both comparisons, ANOVA was followed by Tukey post hoc multiple comparison analysis to determine statistical significance.

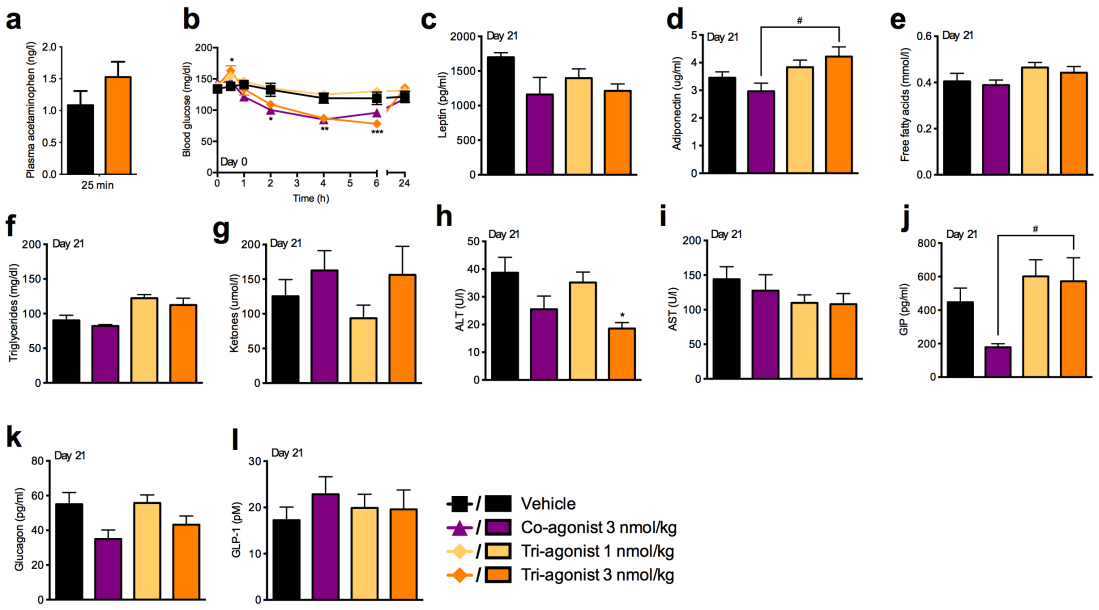


**Supplementary Figure 4. Plasma analysis of DIO mice treated mice (complement to Figure 2).** Effects on **(a)** plasma levels of acetaminophen 25 min. after oral gavage and 40 min. after injection of tri-agonist (3 nmoles per kg body weight). Effects on **(f)** blood glucose following a single bolus injection of compounds. Effects on plasma levels of **(c)** leptin **(d)** adiponectin, **(e)** free fatty acids, **(f)** triglycerides, **(g)** ketone bodies, **(h)** ALT, **(i)** AST, **(j)** total GIP, **(k)** glucagon, and **(l)** total GLP-1 of male DIO mice treated with vehicle (black), a dual incretin co-agonist (purple; 3 nmoles $kg^{-1}$), or a single molecular GLP-1/GIP/glucagon tri-agonist at 1 nmoles $kg^{-1}$ (yellow) or 3 nmoles $kg^{-1}$ (orange). All mice were treated by daily subcutaneous injections. Data in **(a–l)** represent means ± s.e.m. $^{*}P < 0.05$, determined by ANOVA comparing vehicle to compound injections, and $^{\#}P < 0.05$, determined ANOVA comparing dual incretin co-agonist to tri-agonist injections. In both comparisons, ANOVA was followed by Tukey post hoc multiple comparison analysis to determine statistical significance.

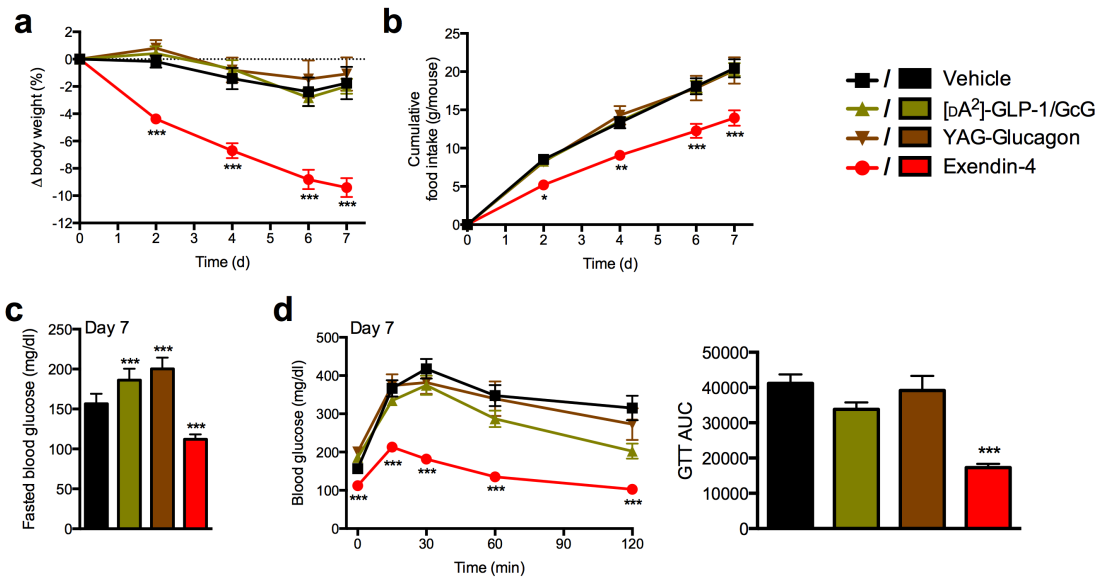


**Supplementary Figure 5. Comparison to other purported triple agonists.** Effects on **(a)** body weight change, **(b)** cumulative food intake, **(c)** fasted blood glucose, and **(d)** glucose tolerance of male DIO mice treated with vehicle (black squares), two different purported GLP-1/GIP/glucagon triple agonists: $_{D}A^{2}$-GLP-1/GcG (olive triangles) and YAG-glucagon (brown triangles), or exendin-4 (red circles). All mice were treated by twice daily subcutaneous injections (separated by 8 hours) at a cumulative dose of 50 nmoles $kg^{-1}$ $day^{-1}$ (2 x 25 nmoles $kg^{-1}$). Data in **(a–d)** represent means ± s.e.m. *$P < 0.05$, ** $P < 0.01$, *** $P < 0.001$, determined by ANOVA followed by Tukey post hoc multiple comparison analysis comparing vehicle to compound injections.

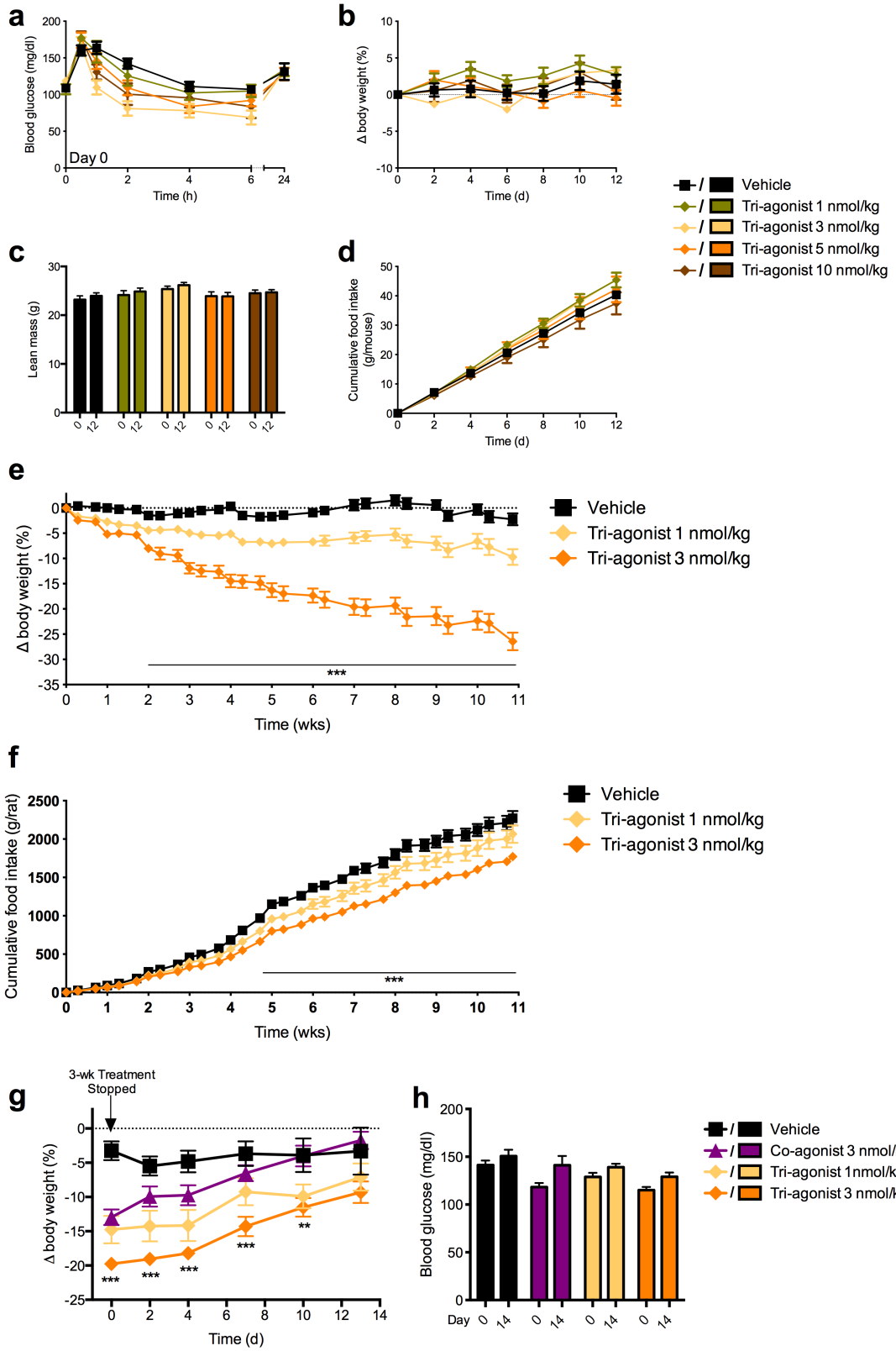


**Supplementary Figure 6. Lack of acute hypoglycemia or long-term adverse effects with tri-agonist treatment.** Effects on **(a)** acute fasted blood glucose, **(b)** body weight change, **(c)** lean mass, and **(d)** cumulative food intake of lean male C57Bl/6 DIO mice (n = 8 per group; age 6 months) treated with vehicle (black squares) or increasing daily doses of the tri-agonist at 1 (olive diamonds), 3 (yellow diamonds), 5 (orange diamonds), or 10 nmoles $kg^{-1}$ (brown diamonds). Effects on **(e)**

body weight change and **(f)** cumulative food intake of DIO Long Evans rats treated 3-times per week with vehicle (black squares) or the tri-agonist at 1 or 3 nmoles $kg^{-1}$ (yellow diamonds and orange diamonds, respectively). Effects on **(g)** body weight regain and **(h)** *ad libitum*-fed blood glucose of DIO male mice two weeks after treatment cessation. All mice were treated daily for 3 weeks with vehicle (black squares), a dual incretin co-agonist (purple triangles; 3 nmoles $kg^{-1}$), or a single molecular the tri-agonist at 1 nmoles $kg^{-1}$ (yellow diamonds) or 3 nmoles $kg^{-1}$ (orange diamonds). Data in **(a–h)** represent means ± s.e.m. *$P < 0.05$, ** $P < 0.01$, *** $P < 0.001$, determined by ANOVA followed by Tukey post hoc multiple comparison analysis comparing vehicle to tri-agonist injections.

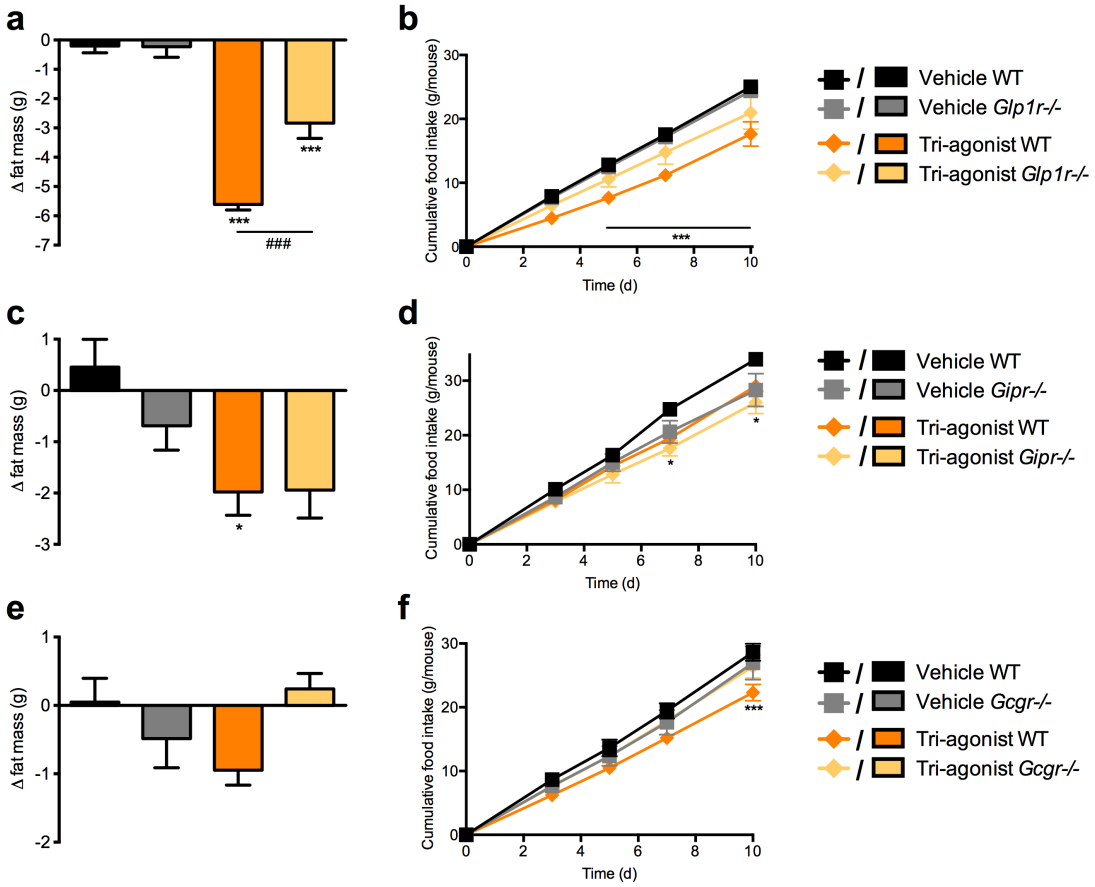


**Supplementary Figure 7. The metabolic benefits of the tri-agonist are blunted in *Glp1r*–/–, *Gipr*–/–, and *Gcgr*–/– mice (complement to Figure 3).** Effects on **(a)** fat mass change and **(b)** cumulative food intake in wild-type or *Glp1r*–/– male DIO mice. Effects on **(c)** body weight change and **(d)** cumulative food intake in wild-type or *Gipr*–/– male HFD mice. Effects on **(e)** body weight change and **(f)** cumulative food intake in wild-type or *Gcgr*–/– male HFD mice. All mice were treated every other day with vehicle (wt: black squares; ko: gray squares) or the tri-agonist (wt: orange diamonds; ko: yellow diamonds) at a dose of 10 nmoles $kg^{-1}$. Data in **(a–f)** represent means ± s.e.m. $^{*}P < 0.05$, $^{**}P < 0.01$, $^{***}P < 0.001$, determined by ANOVA comparing vehicle to compound injections within each genotype, and $^{\#}P < 0.05$, $^{\#\#}P < 0.01$, $^{\#\#\#}P < 0.001$, determined ANOVA comparing treatment of the tri-agonist between genotypes. In both comparisons, ANOVA was followed by Tukey post hoc multiple comparison analysis to determine statistical significance.

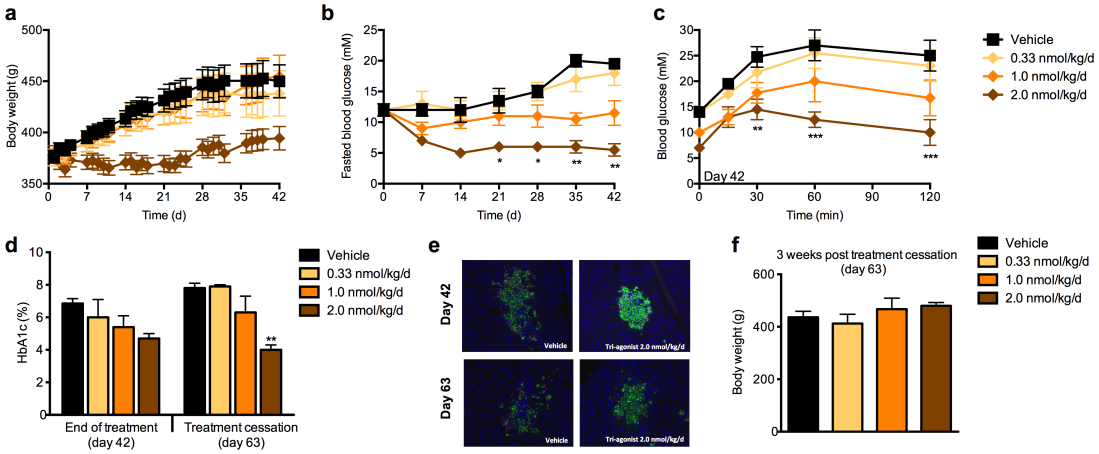


**Supplementary Figure 8. Unimolecular GcgR, GLP-1R, and GIP triple agonism prevent hyperglycemia in ZDF rats.** Effects on **(a)** body weight progression, **(b)** fasted blood glucose, **(c)** intraperitoneal glucose tolerance, **(d)** HbA1c, **(e)** islet cytoarchitecture and immunohistochemistry for insulin (green), glucagon (red), and Dapi staining (blue) following 6-weeks of treatment with escalating doses of the tri-agonist in male ZDF rats (age 9 weeks at start of study). Effects on **(d)** HbA1c, **(e)** islet cytoarchitecture and immunohistochemistry, and **(f)** body weight regain following 3 weeks of compound wash-out and 9 weeks after treatment initiation. Data in **(a–f)** represent means ± s.e.m. *$P < 0.05$, ** $P < 0.01$, *** $P < 0.001$, determined one- or two-way ANOVA followed by Tukey post hoc multiple comparison analysis to determine statistical significance comparing vehicle to tri-agonist injections.